MULTIMODAL NANOPARTICLES FOR CANCER THERAPY AND IMAGING

By

Vanessa Rochelle Bright

Thesis

Submitted to the Faculty of the

Graduate School of Vanderbilt University

in partial fulfillment of requirements

for the degree of

MASTER OF SCIENCE

In

Chemical and Physical Biology

December, 2012

Nashville, Tennessee

Approved:

Wellington Pham, Ph.D.

J. Oliver McIntyre, Ph.D.

C. Chad Quarles, Ph.D.

To Dorothy Wall, my grandmother,

her life was an example of hard work and courage

which I strive to follow.

ACKNOWLEDGEMENTS

I would like to thank my advisor Dr. Wellington Pham, for his continued guidance and support throughout this project. The work would not be possible without his funding of the project; he has taught me a great deal over the course of this work and I have appreciated his effort to teach and train me. Thanks is also due to others I have had the pleasure of working with in our laboratory; Meiying Zhu for her help in a variety of areas. Dr. Mike Nichols and Dr. Don Nolting are greatly appreciated for their training and support in my chemistry work. I thank fellow trainees Dave Abdollahian and Richard McClure for their support of this project. Our collaborator Dr. Sebastian Joyce has been invaluable for his insight into immunology and Dr. Pavlo Gilchuk is appreciated for his training and guidance through immunological techniques. This work relied on Dr. Paul Savage's production of α-GalCer.

This work would not have been possible without financial support from Dr. John Gore's cancer imaging training grant and the support of the Vanderbilt University Institute of Imaging. A warm thanks goes to all those I have enjoyed working with day to day and have found a way to brighten my day. Special thanks go to Nancy Hagans for her willingness to help with administrative matters.

The Chemical and Physical Biology Program has been wonderful to work with. I'd like to thank Dr. Hassane Mchaourab for his willingness to help and his guidance and Lindsay Meyers for her help in any manner needed. My training here would not have been possible but for the financial support of the Chemical and Physical Biology

Admissions Program through my first year of study. The camaraderie of my fellow CPB students has made my time here a joy.

Nobody has been more important to me in the pursuit of knowledge than the members of my family. My parents have provided me motivation and loving support. I would not be here without their guidance and instruction. My brother, Jonathan's example first started my curiosity with science. My sister, Kimberly has loved me as only a sister can. My brother, Zach has provided my life with entertainment while in this program.

TABLE OF CONTENTS

LIST OF FIGURES

Figure

Page

CHAPTER I

Introduction

In this thesis, the power of synthetic chemistry and colloidal nanotechnology will be employed for their use in cell therapy and imaging. A new approach to dendritic cell (DC)-based immunotherapy will be examined. The application of superparamagnetic iron oxide (SPIO) nanoparticles as a delivery vehicle will be explored and preliminary data of the efficacy of this therapy will be presented, prompting further research in this area. In the last part of the thesis, the development of a near-infrared (NIR) dye for amine reactive moieties is described.

Rationale for Thesis

It is a well-known fact that cancer is still a major health concern in modern times. Despite the scientific progress that has been made in treatments for a variety of cancers, the Center for Disease Control still reports cancer as the second leading cause of death in the United States, surpassed only by heart disease (Murphy, 2012). Recently, since 1999, cancer has eclipsed heart disease as the leading cause of death in Americans under the age of 85 (Siegel et al., 2011). Globally, it is estimated that 7.6 million deaths were attributed to cancer in 2008 (Jemal et al., 2011). Since 1991-1992, cancer death rates have failed to meet the extrapolated values expected for mortality rates in the United States, accounting for approximately 649,300 cancer deaths in men that have been

avoided and 248,600 in women, as of 2007 (Siegel et al., 2011). Progress has been made in treatment of and screening for cancer, but much work is yet to be done.

The three cancer types which account for the greatest incidence in men in the United States are prostate, lung and bronchus, and colon and rectum; among women they are breast, lung and bronchus, and colon and rectum (Siegel et al., 2011). It is apparent that epithelial cancers play a large role in the incidence of cancer. In fact, epithelial cancers account for over 85% of all cancers (Backman et al., 2000). Cancer models based in the epithelial tissue are therefore of special importance for preclinical studies of cancer treatments. To that end, a preclinical model of breast cancer is used in our study of a new approach to DC-based immunotherapy.

DC-based immunotherapy is an emerging technique for the treatment of cancer. Since the discovery of DC by Ralph Steinman in 1973 (Steinman and Cohn, 1973), therapies based on the immune activating powers of this cell type have been developed and shown efficacy in both mouse models (Flamand et al., 1994; Grabbe et al., 1991; Mayordomo et al., 1995; Porgador et al., 1996) and the clinic (Hsu et al., 1996). Immunotherapy has shown limited positive results due to the complicated processes of DC preparation and distribution (Martin-Fontecha et al., 2003). We propose improvements to immunotherapy through the use of a nanoparticle delivery vehicle. Nanoparticles are preferentially taken up into DCs due to their size (Hirosue et al., 2010). Conjugation of immune activating biomolecules to a nanoparticle can, therefore, enhance the effectiveness of treatment. There is a dense population of DCs within the lung tissue due to the exposure to the environment (Holt et al., 1993). This fact has spurred us toward the directing immunotherapy agents to the resident DC of the lungs.

Background of Immunotherapy

Features and Function of Dendritic Cells

The discovery and characterization of DCs by Steinman and Cohn in the early 1970s brought to the forefront a new area of research for treatment of cancer, immunotherapy. DCs are bone marrow-derived immune cells that are present in small numbers and can be isolated from other lymphocytes based on lack of Ig and thy-1 and can be practically separated due to the adherent nature of DCs (Steinman and Nussenzweig, 1980). They are professional antigen-presenting cells (APCs) that work to process and present antigens on major histocompatibility complex (MHC) molecules for recognition by cells of the adaptive immune system, such as T-lymphocytes. DCs have multiple roles and dynamically shift phenotypes in response to their environment (Grolleau et al., 2005). The progenitor of DCs is rare in normal blood, just like the DCs themselves, accounting for only 0.1% of the cells (Ema, 1990). Progenitor cells can differentiate into both Langerhans cells (from $CD1a^+$ DCs) and interstitial DCs (from $CD1a^-$ DCs), both being $CD11c^+$ (Ito et al., 1999).

Migration of the DCs to the lymph node (LN) is important for the ability of peripheral DCs to present antigen to cytotoxic T lymphocytes (CTLs) and T-helper-cells (Pham et al., 2009). Immature DCs reside in tissues that are in contact with the external environment, such as the epithelium of the skin, gastrointestinal tract, and respiratory tract as well as other peripheral tissues. There, they scan their surroundings for both self and foreign antigens and pathogen associated molecular patterns (PAMPs), such as

lipopolysaccharide (LPS), acting as a scavenger cell for immune surveillance (Grolleau et al., 2005). Upon encountering these "danger" signals, these DCs undergo a differentiation and maturation process manifested by the up regulation of key factors needed to induce T lymphocyte activation: MHC-I, MHC-II, and costimulatory molecules CD80 and CD86 important to both the innate and adaptive immune responses. In this manner, DCs are capable of presenting tumor antigens and effectively stimulating the immune response, targeted against a tumor (Mohty et al., 2002).

The immature and mature DCs have characteristics specific to each purpose that change upon activation. Immature DCs are characterized by their ability to phagocytosis particles and microbes, macropinocytosis to sample extracellular fluid and solutes, and adsorptive endocytosis propagating surface receptors (Pham et al., 2009). When a DC uptakes an antigen and matures it loses its ability to uptake antigens, its morphology changes to allow high mobility, and increased chemokines are expressed to guide the migration to lymphoid tissue (Winzler et al., 1997).

DCs play a part in innate immunity and adaptive immunity; costimulatory molecules and cytokines, such as IL-12 and IL-10, released by the mature DC work to mediate innate immune response. DCs are also involved in the activation of natural killer (NK) cells through production of IL-2. NK cells in turn work to activate DC maturation. IL-2 production is also important to the adaptive immune system due to its ability to induce proliferation of $CD4^+$ and $CD8^+$ T-cell and B-cells. T-helper-cells that have been activated by DCs also secrete IL-2 and go on to become either Th1-cells, which secrete IFN-γ and activate CTLs, or Th2-cells, which secrete IL-4 and are important to humoral immune response through B-cells (Pham et al., 2009). As can be seen, DCs play a

pivotal part in the immune response, both the innate and adaptive arms. Because of their ability to induce and direct a potent immune response, DCs are considered to be promising tools for immunotherapy.

Dendritic Cell-Based Immunotherapy

The tumor tolerance model in **Figure 1** shows the proper activities (anti-tumor model) of the DCs are inhibited by growth factors and cytokines in the tumor microenvironment, IL-10, VEGF, TGF-β, and IL-6. These factors prevent DCs from differentiating, maturing and migrating. IL-10 specifically inhibits expression of IL-12 and costimulatory molecules needed to activate the immune response and induces T-cell anergy, a state of immune unresponsiveness. All these factors, among others, allow the tumor to escape the immune response (Pham et al., 2009).

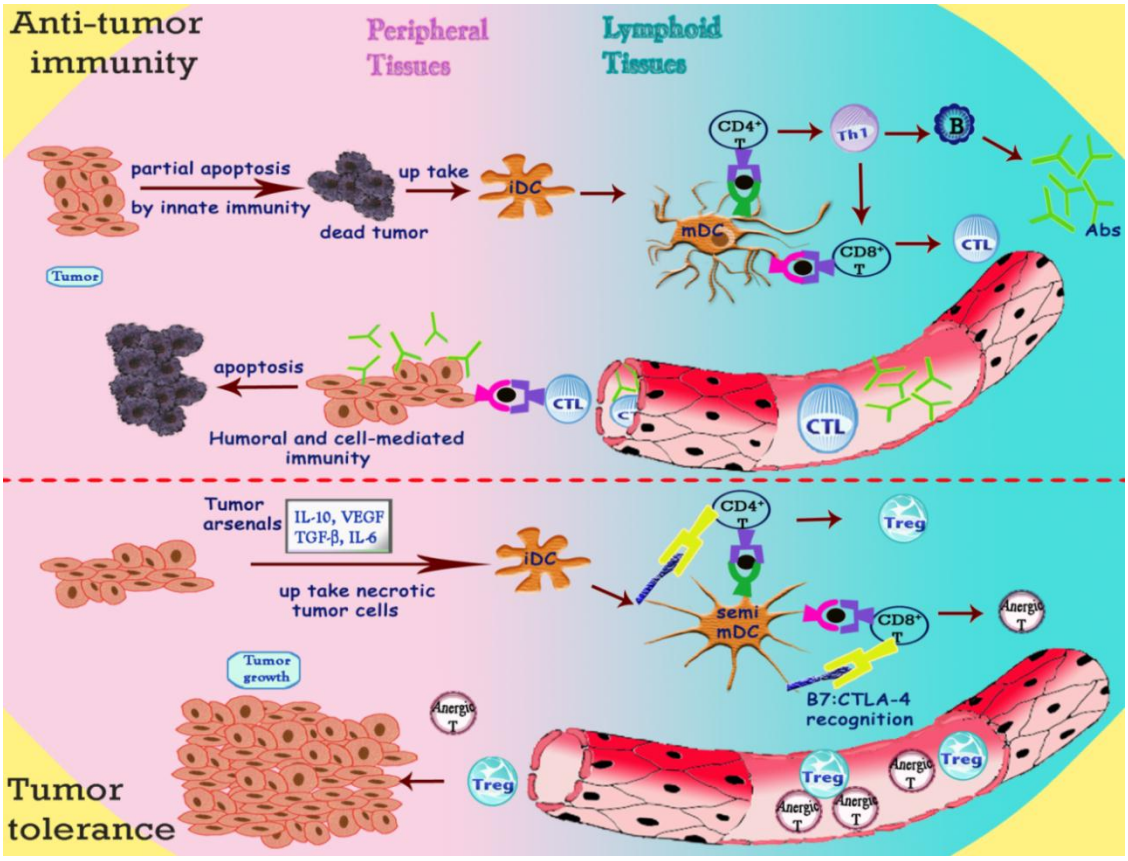

Figure 1. Activity of DCs in antitumor immunity and tumor tolerance. (Pham et al., 2009)

Immunotherapy focuses on this mechanism of tumor tolerance and works to circumvent the tumor arsenal by artificially activating the DCs against the tumor. This is most commonly done through *ex vivo* stimulation of DCs. DCs are isolated from the bone marrow and pulsed with the "danger signal," a tumor antigen. The mature DCs are then adaptively transferred to the patient through infusion where they are able to migrate to the LN and induce uninhibited immune response.

The efficacy of DC-based therapy for cancer treatment was demonstrated successfully with various mouse tumor models (Flamand et al., 1994; Grabbe et al., 1991; Mayordomo et al., 1995; Porgador et al., 1996). This technique was first translated into

clinical therapy for the treatment of follicular B cell lymphoma in 1996 (Hsu et al., 1996). In that work, patients received tumor-specific idiotype protein-pulsed DCs via infusion. The result of that first clinical trial demonstrated that 8 out of 10 patients developed a proliferative cellular response to idiotype protein. Among those, two patients had partial tumor regression. Encouraged by that study, a large number of DC-based clinical trials have been pursued for the treatment of melanoma (Thurner et al., 1999), prostate cancer (Fong et al., 2001; Lodge et al., 2000), colorectal cancer (Nair et al., 2002), gastrointestinal cancer (Sadanaga et al., 2001), breast cancer (Brossart et al., 2000), and renal carcinoma (Holtl et al., 1999; Kugler et al., 2000). Despite significant advancements in DC-based therapy, it has been challenging to develop a simple yet robust method for activating the immune system against cancer with antigen-activated DCs. To date, numerous distribution methods have been applied; however, their effectiveness has been limited by the complicated processes of DC preparation and distribution, and the small percentage of DCs that migrate to the LNs (Martin-Fontecha et al., 2003).

Background of Chemical Probes in Imaging

Development of chemical probes for imaging is important to cancer research for a variety of reasons. Chemical probes for molecular imaging can be used to study many aspects of cancer biology. The most obvious use of imaging techniques is for detection of a disease by image anatomical features of cancer itself. The use of chemical probes allows imaging of not only anatomy, but also visualization of expression and activity of specific molecules and biological processes that influence tumor behavior and/or

response to therapy (Weissleder, 2006). Molecular probes may also be used to screen preclinical drug discovery, therapeutic assessment and validation of disease biomarkers (Nolting et al, 2012). Molecular imaging can be used to answer the questions of where a tumor is located and its size, as well as, tracking the spread to LNs and metastases, and information that may warrant altering treatment strategy (Weissleder, 2006). Computed x-ray tomography (CT), magnetic resonance imaging (MRI), ultrasound (US), nuclear magnetic resonance (NMR), and optical imaging contribute to the study of cancer as traditional anatomical imaging methods as well as for molecular basis of disease (Jaffer and Weissleder, 2005). Use of a magnetic nanoparticle MRI contrast agent has been able to detect millimeter sized nodal metastases (Harisinghani et al., 2003). Resolution of this size demonstrates how powerful molecular imaging is for the detection of cancer and monitoring growth. Cancer treatment can be monitored through detection of growth and metastases, but also through targeting biological process such as apoptosis and angiogenesis. [18F]fluorodeoxyglucose (FDG) positron emission tomography (PET) can be used to monitor treatment response through cell growth and death (Weissleder, 2006). Drug development can also be impacted by molecular probe imaging through target discovery and identifying new efficacy endpoints. "There is an opportunity to apply combinatorial methods, chemical biology, synthetic small molecule compounds, and newer nanomaterials as scaffolds to improve pharmacological behavior (Weissleder, 2006)." In this thesis two chemical imaging probes will be discussed, the use of SPIO nanoparticles and the synthesis of a targeting NIR dye.

CHAPTER II

Superparamagnetic Iron Oxide Nanoparticle Probe for Immunotherapy

Rationale

Within the realm of immunotherapy, mucin 1 (MUC1) is a highly studied protein for use as an immunological target. Tumor antigens derived from the MUC1 protein are one of the most frequently tested in DC-based clinical trials (Kobukai et al., 2011). The NCI Translational Research Working Group has prioritized MUC1 as second among 75 tumor-associated antigens in regards to therapeutic function, immunogenicity, role of Ag in oncogenicity, specificity, expression level, stem cell expression, percentage of patients with antigen positive cancer, and cellular location (Cheever et al., 2009). The MUC1 tumor antigen is, therefore, ideal for the testing of a novel delivery system.

MUC1 is a transmembrane protein specific to epithelial tissue; the heterodimer from the mucin family of molecules containing a solely extracellular subunit and a subunit containing a short extracellular stem, a single transmembrane domain, and the cytoplasmic tail (Hattrup and Gendler, 2006). The extracellular component is composed of a variable number of nearly perfect 20 amino acid tandem repeats (TRs) surrounded by five proximal and two distal imperfect repeats. Serine and threonine residues along these repeats provide sites where the protein can be O-link glycosylated to GalNAc (Kinlough et al., 2011). The sequence of the TRs is PDTRPAPGSTAPPAHGVTSA (Vlad et al., 2004). MUC1 differs between normal and cancerous cells both in glycosylation of the TRs and location. Specifically in cancerous tissue the protein is underglycosylated.

Differences can also be seen in the sites of glycosylation and in the O-glycan structure (Taylor-Papadimitriou et al., 1999) with shorter and fewer oligosaccharides. In normal epithelial cells MUC1 is expressed on the apical surface of the ducts and glands, but is overexpressed throughout cells in the tumor mass (Mukherjee et al., 2003).

The MUC1 protein is overexpressed in many epithelial cancer types. In addition, the protein is aberrantly glycosylated in 90% of human breast cancers (Pinkhasov et al., 2011), 90% of pancreatic tumors (Dwyer et al., 2006), and >70% of human colon cancer (Mukherjee et al., 2007), as well as high levels in lung, prostate, stomach, and ovary tumors (Mukherjee et al., 2003). Presence of overexpressed MUC1 has been correlated to aggressive cancer phenotypes and an advantage over normal MUC1 expressing cell types (Dwyer et al., 2006). Cancers which have increased expression of MUC1 are more resilient to cytotoxic and oxidative agents (Hattrup and Gendler, 2006).

MUC1 antigens have been studied in preclinical and clinical trials for DC-based immunotherapy to treat multiple epithelial cancers. Differences can be seen in the techniques used to place MUC1 antigen in the DCs as well as in the type of cancer tissue treated. A murine preclinical study tested the ability of DCs transfected with MUC1 RNA, to express MUC1 Ag, costimulatory, and adhesion molecules, to mount an immunological response against MC38 adenocarcinoma cells stably transfected with MUC1 cDNA. MUC1 was expressed in the LNs of the immunized mice as compared to the control treated with nontransfected DC. Humoral and CTL response was seen and vaccination of mice was able to prevent the growth of MC38/MUC1 tumors (Koido et al., 2000). A clinical study looked at the ability of DCs pulsed with two 9-mer MUC1 peptides to treat metastatic breast or ovarian cancer. Of the four MUC1 treated patients,

one had regression of multiple subcutaneous lesions after production of $CD8^+$ and $CD4^+$ T cells. Two other patient's disease was stabilized by the immunotherapy (Brossart et al., 2000). In another study, four out of 10 patients treated saw an immunological response, as indicated by an increase in $CD8^+$ T cells, although only one patient saw a stabilization of tumor growth (Pecher et al., 2002). Immunological and clinical response has been seen in advanced metastatic breast and ovarian cancers when treated with MUC1 epitope pulsed DCs (Wierecky et al., 2006). Twenty patients with unresectable or recurrent pancreatic cancer were treated with DCs pulsed with a 100-mer peptide from the TR domain. Intradermal injections of the MUC1-DCs were given concurrently with intravenous injections of MUC1-CTLs, CTLs stimulated by a MUC1-expressing human pancreatic cancer cell line, YPK-1, to improve a previous study done with MUC1-CTLs alone. Five of the 20 patients had a stabilization of disease while one had a complete response (Kondo et al., 2008). Metastatic breast, pancreatic and papillary cancer has been treated in clinical trials with DCs transfected with plasmid pCMV MUC1 (cDNA of 22 repeats of the mucin TR). Our lab has chosen to focus on the treatment of a mammary epithelial tumor cell line C57MG which has been transfected with MUC1 with a 30-mer antigen from the TR portion of the protein.

Previous work in our lab (Kobukai et al., 2011) has studied DC-based therapy with the use of MUC1 antigen. The use of a delivery molecule, myristoylated polyarginine 11-mer peptide ($MPA_{11}P$), in antigen uptake was analyzed. A previous study (Pham et al., 2007) determined the need for a $MPA_{11}P$ for *in vitro* uptake of a fluorescence probe to DCs. The 30-mer antigen (APDTRPAPGSTAPPAHGVTSAPDTRPAPGS) and the same antigen covalently

bonded to the $MPA_{11}P$ ($MPA_{11}P$(C14-$(R)_{11}$)-APDTRPAPGSTAPPAHGVTSAPDTRPAPGS) were compared in their ability to induce $CD8^+$ T cells and inhibit tumor growth. DCs were isolated from the bone marrow of C57BL/6 mice for use in the *in vitro* studies. Three groups of DCs were formed, the first were not pulsed with any antigen, the second group was pulsed with MUC1 peptide, and the third which was pulsed with MUC1-$MPA_{11}P$. The DCs were injected subcutaneously in the footpads of C57MG.MUC1 tumor-bearing mice 8 to 10 days post inoculation when the tumors had reached approximately 0.4 cm. A boost was given subcutaneously 10 days after the first injection. Both MUC1 and MUC1-$MPA_{11}P$ pulsed DCs induced $CD8^+$ T cell proliferation at 5 days after DC injection, determined by flow cytometric analysis. The tumor burden was measured using high-resolution US. As can be seen in **Figure 2** antigen-pulsed DCs inhibit the growth of the C57MG-MUC1 tumors. Addition of the $MPA_{11}P$ delivery molecule inhibits tumor growth to a greater degree than the MUC1 alone.

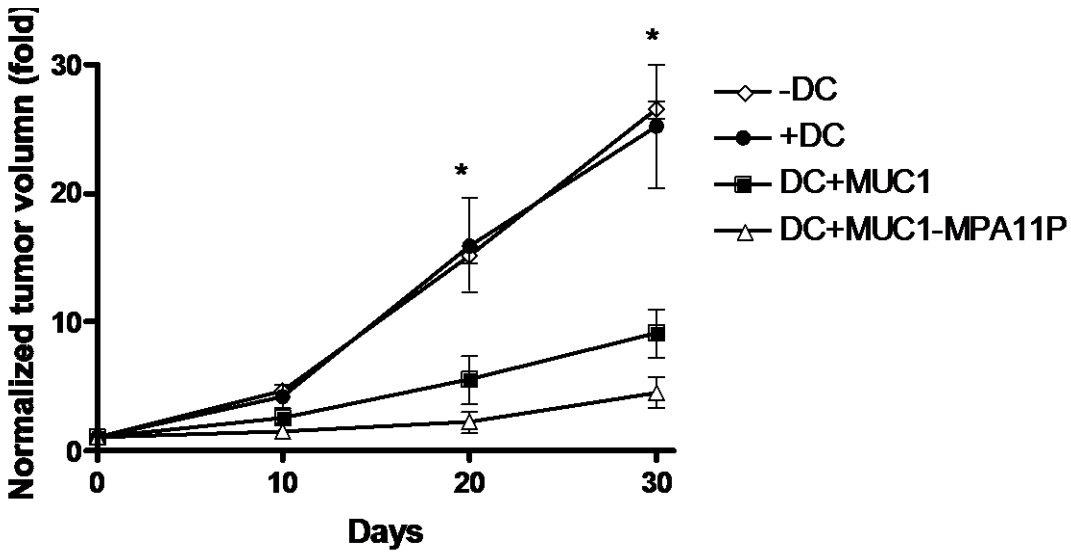

Figure 2. The tumor growth was monitored, measured, and compared with the original size (day 0) using high-resolution US. Each point represents a mean of six measurements. A modest reduced tumor growth was observed with MUC1-stimulated DCs (DC + MUC1), and there was a significant difference in the groups of mice treated with DC + MUC1-$MPA_{11}P$ compared with those treated with DC + MUC1. *P < .05 (DC + MUC1-$MPA_{11}P$ vs. DC + MUC1). (Kobukai et al., 2011)

The addition of a delivery vehicle increases the effectiveness of the immunotherapy, indicating that increased uptake of the antigen can be mediated by conjugation to a molecule that is readily endocytosed. Along with delivery molecules such as $MPA_{11}P$, nanoparticles are known to taken up by DCs (Hirosue et al., 2010). Conjugation of antigen to nanoparticles have the potential to be delivered increasingly well into DC and induce an immune response. Nanoparticles have the added advantage over $MPA_{11}P$ type delivery molecules of multivalency. Nanoparticles have the ability to conjugate to a variety of biomolecules, allowing for versatility in design as a delivery molecule.

Methods and Results

Delivery Molecule Design

Design of an ideal carrier molecule takes into consideration a variety of characteristics. The size of the molecule is important; nanoparticles are molecules that have a particularly desirable size to be taken up by DCs. Specifically nanoparticles that are smaller than 45 nm in diameter have been shown to target resident DCs within the LNs and when coupled with a protein were able to induce humoral and antigen-specific $CD8^+$ T cell responses (Hirosue et al., 2010). Biocompatibility is also important, a molecule must be nontoxic and able to be processed and flushed out of the body without any harmful byproducts. The third important characteristic is the ability of the molecule to be conjugated to the antigenic peptide, preferably the ability to conjugate a variety of molecules.

Superparamagnetic iron oxide nanoparticles

The SPIO nanoparticles are useful as a delivery vehicle due to the multivalency, biocompatibility, as well as the added ability to track the particles through MRI. Dextran-coated iron oxide nanoparticles produced in our lab are found to have a mean diameter of approximately 30 nm (**Figure 3**), within the ideal size for a delivery molecule. The dextran surface can be modified using an epoxy amine linker to produce an easily conjugated amine surface. Since SPIO nanoparticles have been used as a contrast agent for MRI the toxicity of the nanoparticle has been studied in both mice and humans. In mice, SPIO nanoparticles are not known to cause toxicity. SPIO

nanoparticles are seen to distribute to the heart, spleen, liver, lung, kidney, and brain then eliminated quickly without pathology. In both single and repeated dosing little nanoparticle buildup is seen (Liu, 2008). In humans, acute toxicity of SPIO nanoparticles have been found to be comparable to clinically approved infused intravenous contrast agents and there is no evidence that use of SPIO nanoparticles as a contrast agent causes kidney damage (Winer et al., 2011).

DCs have been shown to be able to uptake iron oxide nanoparticles. Previous work in our lab (Kobukai et al., 2010) used polylysine as a transfecting reagent to mediate the uptake into DCs, although a study by de Vries et al. showed that SPIO nanoparticles can be taken up without the need of a delivery agent, requiring a longer incubation time (de Vries et al., 2005). The longitudinal and transverse relaxation rates (R_1 and R_2, respectively) of SPIO nanoparticles can be seen in **Figure 3.** The R_2/R_1 ratio is high making them suitable for T_2-weighted imaging.

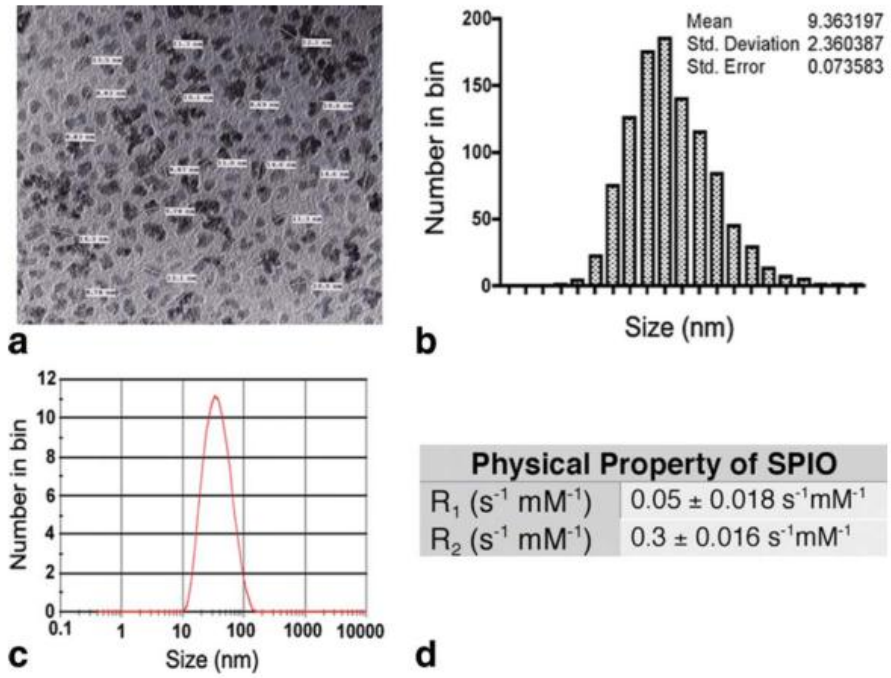

Figure 3. Physical properties of the synthesized dextran-coated SPIO particles. a: TEM image of the SPIO nanoparticles. b: The distribution of the iron core calculated from the TEM image. c: The overall size of dextran-coated SPIO particles measured by a Zetasizer. d: The R values. (Kobukai et al., 2010)

The SPIO nanoparticles consisting of an iron oxide core and dextran coating were produced from The Pham Laboratory (Kobukai et al., 2010). A saturated mixture of dextran and ferric chloride was coalesced with a ferrous chloride solution at room temperature. The pH was elevated to 10 via drop wise addition of an ammonium hydroxide solution. The resulting solution was stirred for several hours. Using deionized water, synthesized particles were separated from the starting materials and dialyzed into a buffer containing normal physiologic concentrations of sodium citrate and sodium chloride.

Epoxy amine linker

As mentioned previously the hydroxyl surface of the dextran-coated SPIO nanoparticles must be modified due to the poor nucleophilicity of the surface alcohols. To this end, a linker was developed by our lab consisting of an epoxide terminus and an amine terminus. The short five carbon linker's epoxide terminus is able to react easily with the alcohol groups on the surface of the dextran coated nanoparticle. The amine terminus of the linker is then presented on the surface of the nanoparticle.

Synthesis followed the scheme shown in **Figure 4** and published by Nickels et al (Nickels et al., 2010). The intermediate 5, Pent-4-en-1-aminium 4-methylbenzenesulfonate was developed from our group, it was produced from 5-bromopent-1-ene through a Gabriel synthesis followed by protection of the terminal amine group as an alkenylammonium salt. The alkenylammonium salt prevents the oxidizing of the amine in the next step as well as by nucleophilic attack of the amine on the epoxide ring.

A dimethyldioxirane solution of was made fresh as follows: acetone (39.0 mL, 531 mmol), sodium bicarbonate (36.0 g, 429 mmol), and water (60 mL) were added to a 500 mL three-neck round bottom flask, which was fitted with a solid addition funnel, nitrogen inlet and Vigreux column. Attached to the Vigreux column was a 100 mL two-neck round bottom flask equipped with a dry-ice condenser, which as then attached to a house vacuum line equipped with an inline vacuum trap. Nitrogen was used to purge the entire system. Oxone® (75.8 g, 123 mmol) was added slowly to the reaction mixture via the solid addition funnel over a period of 1.5 hours with constant stirring and a steady flow of nitrogen. After addition of Oxone® the entire system was put under the house

vacuum for a period of 2 hours. Dimethyldioxirane in acetone (23 mL, 0.099 M) was trapped in the two-neck round bottom flask, which was subsequently sealed and stored in a freezer until needed.

To a dry 100 mL round bottom flask were added pent-4-en-1-aminium 4-methylbenzenesulfonate (0.352g, 1.37 mmol) and dry CH_2Cl_2 (10.0 mL), which was then cooled to 0 °C under an atmosphere of nitrogen. The freshly prepared dimethyldioxirane solution (23.0 mL, 2.28 mmol) was added slowly, and the resultant clear reaction mixture was stirred at 0 °C for a period of 1.5 hours, then at 4 °C overnight. The solution was added to dry diethyl ether (150 mL), which produced a white precipitant. The precipitate was filtered and rinsed with additional cold diethyl ether then dried under high vacuum producing the final product, the epoxy amine linker (8) as a white solid (0.334 g, 89.4% yield).

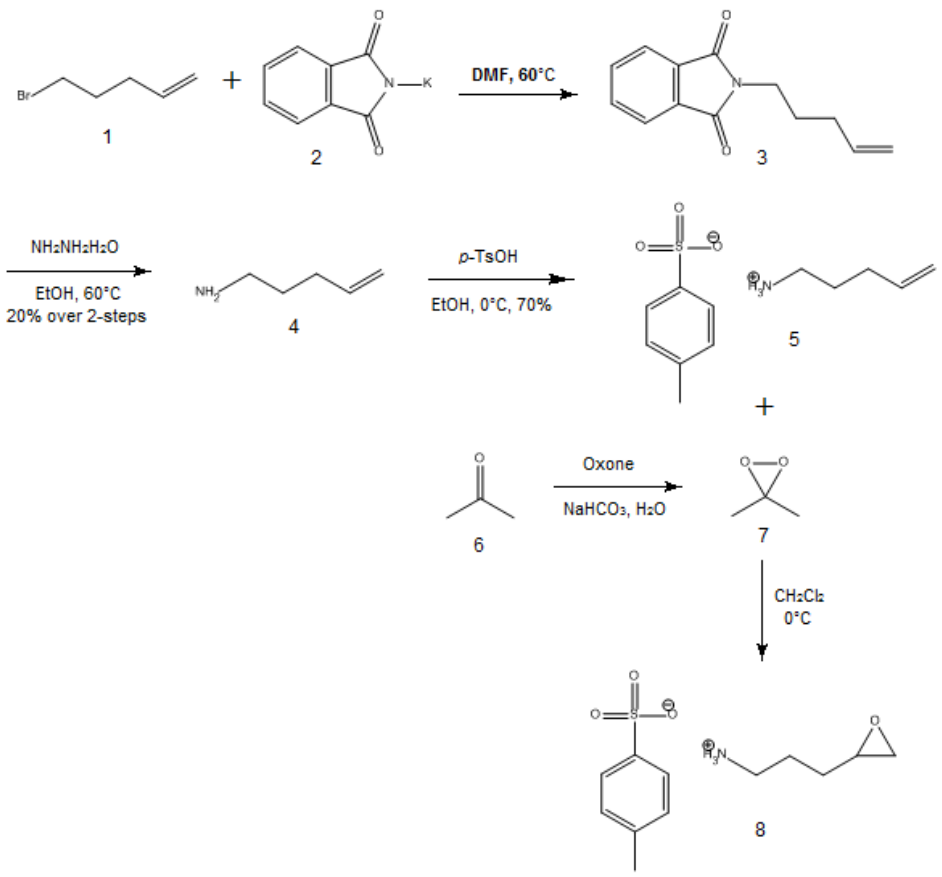

Figure 4. Design and syntheses of epoxy amine linker for functionalizing nanoparticles (Adapted from The Pham Laboratory).

The product was verified by ^{1}H NMR in $CDCl_3$ using a Bruker 300 MHz and peaks were assigned based on the epoxy amine linker (**Figure 5**).

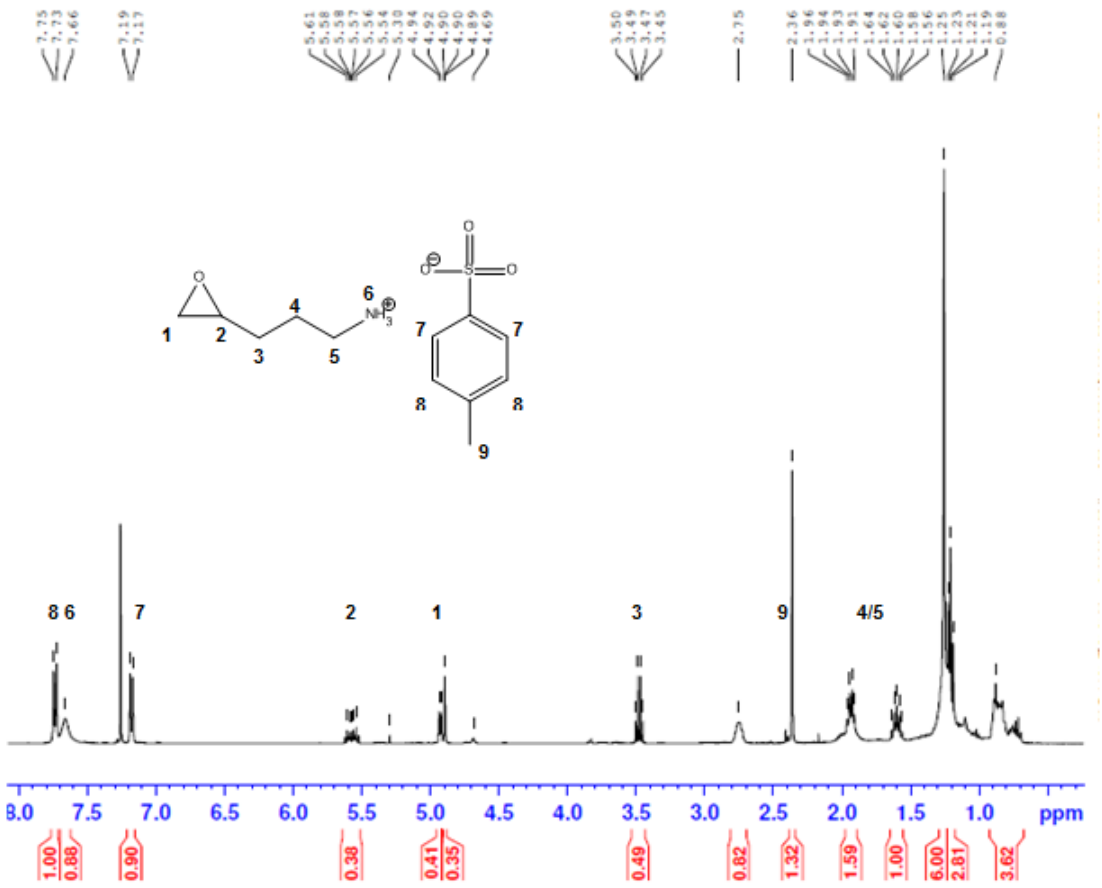

Figure 5. ^{1}H NMR of epoxy amine linker product.

Coating the nanoparticle with an epoxy amine linker

The epoxy amine linker was coupled to the SPIO nanoparticle as seen in **Figure 6**. The nanoparticles were prepared as described above and resuspended in phosphate buffered saline (PBS) at 11 mg/mL of iron. The epoxy amine linker (35.4 mg, 129 mmol) was dissolved in the nanoparticle solution (2mL, 22 mg), producing a solution with approximately 500 times excess epoxy amine linkers (the number of molecules vs. particles). The reaction was performed overnight, at room temperature, with gentle stirring. Excess free epoxy amine linker was removed from the nanoparticles using PD-

10 desalting column (GE Healthcare, Pittsburgh, PA) following the manufacturer's recommended procedure.

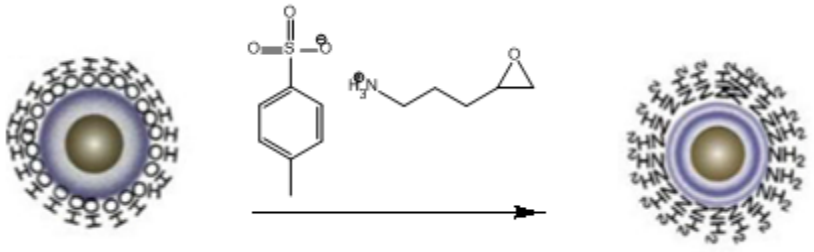

Figure 6. Functionalization of dextran-coated iron oxide nanoparticles with an epoxy amine linker resulting in approximately 40–60 amines on the surface measured with fluorescamine. (adapted from Pham Laboratory)

Use of *N*-succinimidyl 3-(2-pyridyldithio) propionate linker

The amine surface of the SPIO nanoparticle allows for easy conjugation of a biomolecule through a crosslinker. The design of conjugation takes into account the need for release of the biomolecules once inside the DCs. The reductive environment of trafficking within the cell can be exploited by inclusion of a reduction-sensitive conjugation, such as a disulfide bond. Use of reducible conjugation has enhanced efficacy in intracellular targeting of biomolecules with a synthetic carrier (Hirosue et al.; van der Vlies et al., 2010). N-succinimidyl 2-(2-pyridyldithio) propionate (SPDP) is a short-chain crosslinker containing a disulfide bond. The heterobifunctional reagent has an *N*-hydroxysuccinimide (NHS) ester terminus and a 2-pyridyl disulfide terminus. The NHS-ester reacts easily with amine groups; the 2-pyridyl disulfide reacts with thiols (Carlsson et al., 1978), found in peptides containing cysteine. SPDP is a commercially

available linker through Thermo Scientific as described in Carlsson et al (Carlsson et al., 1978).

Conjugation with SPDP was done following the procedure in the reagent instructions and indicated in **Figure 7**. A 20 mM solution of SPDP reagent was formed by dissolving 2 mg of SPDP in 320 µL of dimethyl sulfoxide (DMSO). Amine containing nanoparticle (5mg) was dissolved in PBS (1.0 mL) to which was added 25 µL of the 20 mM SPDP solution. After the reaction was left at room temperature for 30 minute nonreacted SPDP was removed with an equilibrated disposable PD-10 desalting column (GE Healthcare, Pittsburgh, PA). The column had been equilibrated according to manufacturer's instructions with 25 mL of PBS. Sulfhydryl containing biomolecule (3 mg) was added to the collected solution and incubated overnight at room temperature. The reaction was confirmed by UV-vis Spectrophotometer (Agilent Technologies, Santa Clara, CA) showing a peak at 343 nm (the absorbance of the Pyridine 2-thione byproduct).

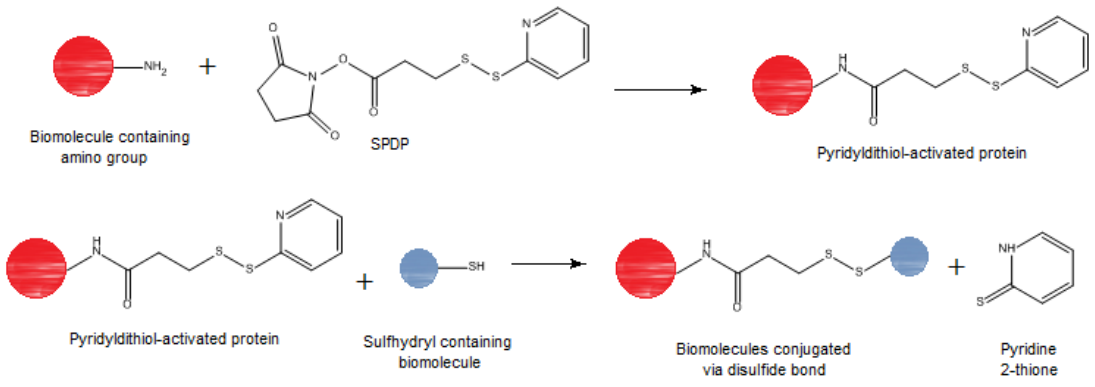

Figure 7. Reaction scheme for conjugation of amine and thiol containing biomolecules.

Bioconjugation of SPIO Nanoparticle

α-GalCer as adjuvant

As immunotherapy has become more studied it has become apparent that activating the immune system with antigen alone is not very efficient. A successful cancer vaccine should work in multiple ways to activate the immune system, especially simultaneous activation of both the innate and adaptive arms of the immune system (Lakshminarayanan et al.). Inclusion of an innate immune adjuvant is a technique used to enhance efficacy of therapy (Mukherjee et al., 2007). α-Galactosylceramides (α-GalCer) are a family of immunostimulants developed form a natural product of an Okinawan marine sponge (Franck and Tsuji, 2006). The natural product, as well as, the synthetic material, KRN7000, activates immunity through natural killer T (NKT) cells. NKT cells are innate lymphocytes that have phenotypic and functional properties of both NK cells and T cells (Franck and Tsuji, 2006). After endocytosis by APCs, α-GalCer is presented on the cell surface by CD1d gene family to NKT cells (Morita et al., 1995; Zhou et al., 2002). Activated NKT cells give a boost to the innate and adaptive immune cells: NK cells, macrophages, DCs, $CD4^+$ and $CD8^+$ T cells, both through release of cytokines and direct cell-to-cell contact (Thapa et al., 2009). Thereby, α-GalCer can increase the efficiency of DC-based therapy. The adjuvant family is varied by fatty acid chain modifications, many variations have been found to be active (Franck and Tsuji, 2006). Soluble α-GalCer successfully inhibits primary tumor formation in multiple murine sarcoma and carcinoma lines (Hayakawa et al., 2003). Clinical trials indicate that α-GalCer pulsed DCs are able to activate NKT cells against cancer in humans, albeit to a

lesser degree than in murine models. This therapy significantly increased antigen specific, interferon (IFN)-γ-producing, and memory T cells when given prior to an inactivated influenza vaccine in one patient (Chang et al., 2005). Injection of soluble α-GalCer has been demonstrated to cause anergy of the NKT cells, an intrinsically functional inactivation due to strong T-cell receptor signals delivered in the absence of costimulation. This can be avoided by loading mature DCs with α-GalCer *in vitro* (Sullivan and Kronenberg, 2005) or by conjugating the adjuvant to a nanoparticle (Thapa et al., 2009). A study by Reddy et al. showed that by conjugating an adjuvant to a nanoparticle it is possible to activate an immune response without pulsing DCs *ex vivo* (Reddy et al., 2007). The α-GalCer used for our studies, seen in **Figure 8**, is modeled from KRN7000, with modification to the fatty acid chain, shortened by two methyl groups, and the hydroxymethyl group, providing an accessible thiol.

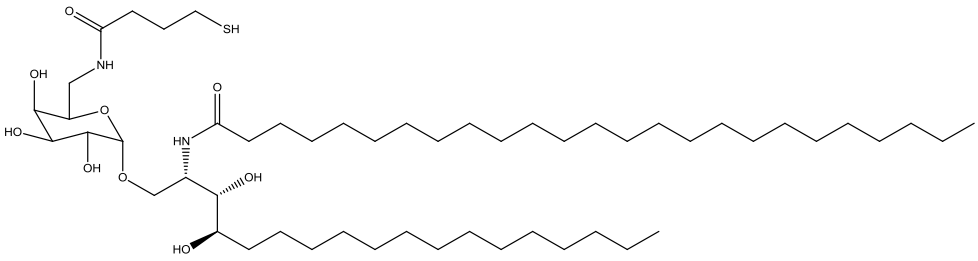

Figure 8. Structure of thiolated α-GalCer.

Conjugation of α-GalCer to aminated SPIO nanoparticle using the SPDP crosslinker proceeded as previously described and shown in **Figure 7**. Due to relatively poor solubility in organic and aqueous solvents, glycolipids are often dissolved in DMSO and then diluted in the solvent of choice (Liu et al., 2006). The thiolated α-GalCer was

provided in a 1 mg/mL solution of DMSO. Working as the sulfhydryl containing biomolecule, 100 μL of the α-GalCer solution were added to the pyridyldithiol-activated SPIO nanoparticles. The product was monitored by analyzing its absorbance at 343 nm on the UV-vis Spectrophotometer (Agilent Technologies, Santa Clara, CA).

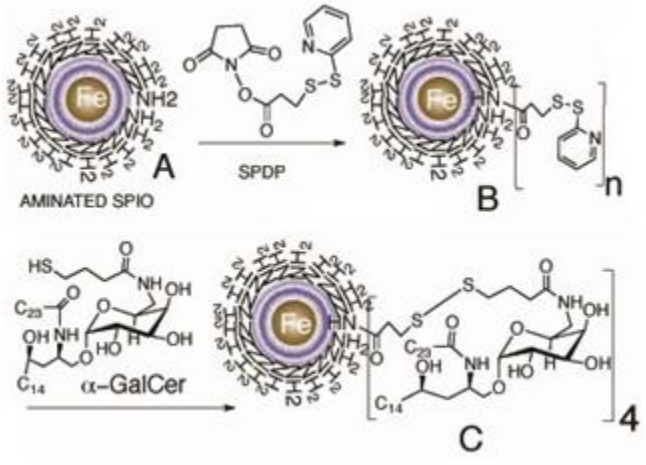

Figure 9. Scheme of conjugation of thiol modified α-GalCer to aminated SPIO nanoparticles. The amino groups on the surface of SPIO nanoparticles (A) were allowed to react with a SPDP crosslinker. The pyridyldithiol-activated SPIO nanoparticles (B) was left in the presence of thiolated α-GalCer to produce a SPIO-α-GalCer conjugate (C) (adapted from Pham Laboratory).

To test the efficacy of the α-GalCer conjugated SPIO nanoparticles, an experiment was done *in vivo* comparing the immune response to that of soluble α-GalCer. Wild-type C57BL/6 mice were injected subcutaneously with varying concentrations of either α-GalCer conjugated to SPIO nanoparticles, soluble α-GalCer, or SPIO nanoparticle alone. After 4 hours blood was collected and the sera isolated and analyzed for IL-4 concentration using an ELISA. The cytokine production is reported in **Figure 10**.

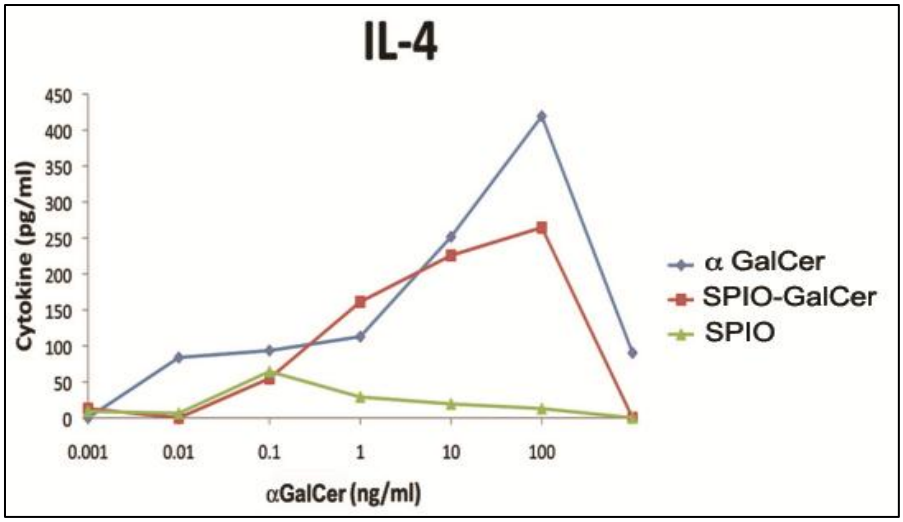

Figure 10. IL-4 production as a measure of immune response after injection of adjuvant laden nanoparticles, nanoparticles alone and adjuvant alone. Conjugation of the adjuvant to the nanoparticle increases activation of the immune response at 1 ng/mL concentration.

α-GalCer does not lose its efficacy for inducing an immune response when conjugated to a nanoparticle. Comparable IL-4 activation can be seen within a 0.1 to 100 ng/mL concentration with a particular advantage to the nanoparticle conjugated adjuvant around 1 ng/mL concentration of α-GalCer.

Synthesis of MUC1, α-GalCer conjugated SPIO nanoparticles

The SPIO nanoparticles provide an opportunity to present multiple molecules as antigens to the immune system simultaneously. In this direction, we propose the development of a particle which is bound to both tumor antigen and the glycolipid molecule α-GalCer. Conjugation of the nanovaccine was accomplished with two reactions of the SPDP crosslinker following the scheme in **Figure 11**. First the 31-mer MUC-1 peptide (APDTRPAPGSTAPPAHGVTSC) was conjugated, followed by

conjugation of the thiolated α-GalCer (1mg/mL in 10% methanol (MeOH) in tetrahydrofuran (THF)).

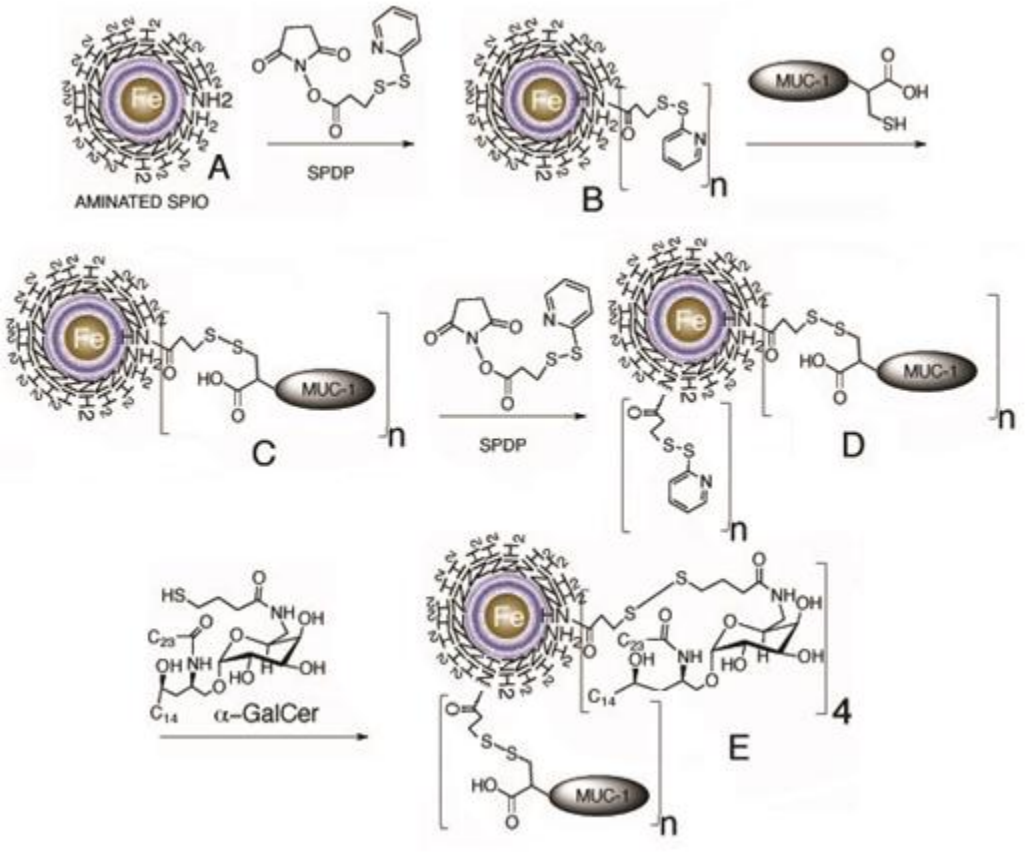

Figure 11. Scheme for conjugation of the MUC1 antigen and α-GalCer glycolipid to SPIO nanoparticles. The amino groups on the surface of SPIO nanoparticles (A) were allowed to react with a SPDP crosslinker. The pyridyldithiol-activated SPIO nanoparticles (B) was left in the presence of cysteine containing MUC1 to produce a SPIO-MUC1 conjugate (C). Similarly the conjugate was again reacted with SPDP to produce more activated linkers on the surface of the nanoparticle (D) which bound to the thiol containing α-GalCer to form a SPIO-MUC1,α-GalCer nanovaccine (E) (adapted from Pham Laboratory).

The absorbance of the solution was measured prior to and follow the addition of α-GalCer or MUC1. The release of pyridine-2-thione could be monitored by the absorbance at 343 nm and the quantity of conjugated molecules could be calculated using

Beer's law, A = εbc, where A is the absorbance, ε is the molar extinction coefficient (8.08 x 103 M-1cm-1 for pyridine-2-thione), b is the path length of the sample (1 cm), and c is the concentration. For MUC1 conjugation the average change of absorbance was 0.1282 AU indicating that 3 x 10^{-8} moles of pyridine-2-thione was released and replaced by MUC1, 2.6 % of the MUC1 added to the solution. In the case of α-GalCer the average change of absorbance was 0.0187 AU indicating that 1 x 10^{-7} moles of α-GalCer had replaced pyridine-2-thione, 8.7% of the α-GalCer that was added to solution.

Treatment of C57MG.MUC1 tumors

A preliminary study was done in a murine model of a MUC1 cancer to ascertain the *in vivo* activity of our nanovaccine. To test the nanovaccine, adult MUC1 transgenic mice were implanted with MUC1-transfected C57MG tumors. The tumor antigen- and adjuvant-conjugated nanoparticle was delivered to the mice via subcutaneous injection. Tumor growth in the treated and untreated groups of mice was measured by US over a 5-week period.

One million C57MG.MUC1 cells in 200 μL serum-free Dulbecco modified Eagle medium were injected subcutaneously into the left mammary fat pad of MUC1 transgenic (MUC1.Tg) mice which were available in our colonies (n = 5). Seven days after inoculation tumors were measured with a caliper to be approximately 0.4 cm and the therapy began (day 0). Three mice (treatment) were immunized with 20 μL of approximately 2 mg/mL SPIO-(MUC1, α-GalCer) in PBS by subcutaneous injection into the footpads three times per week. Tumor size in both the treatment and control group was measured twice weekly with a caliper along the largest diameter of the tumor (every

third measurement is reported in **Figure 12**). None of the tumors reached 10% of the body weight during our 5-week study.

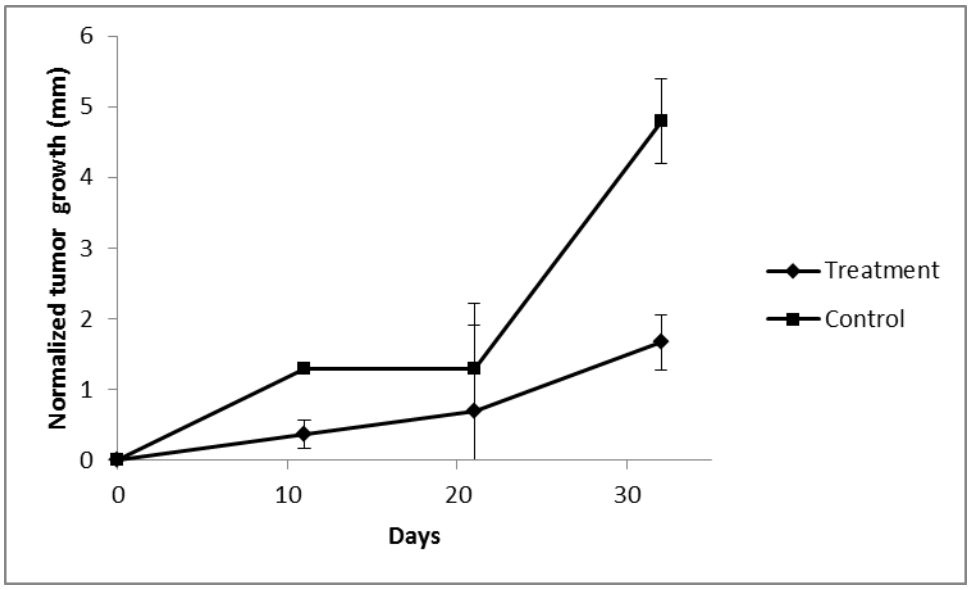

Figure 12. The tumor growth was monitored, measured, and compared with the original size (day 0) using a caliper. Each treatment point is the average of three mice, each control point is the average of two mice. Error bars show one standard deviation.

Tumor growth in the MUC-1 treated mice was inhibited as compared to the non-treated group. In order to analyze further the treatment using the nanovaccine, cytokines produced during immune responses were measured. Injection of the nanovaccine is expected to induce an immune response as it's mechanism of tumor growth inhibition. The cytokine production was measure with an ELISA for INF-γ of the mouse serum. 6 hours after the first treatment, blood was collected from each mouse. The serum was isolated by centrifuge. A sandwich ELISA assay was done of the sera using Rat α-mouse IFN-γ antibodies detected by avidin peroxidase and visualized with TMB substrate

according to BD Biosciences protocols. The concentrations calculated from the standard curve are shown in **Figure 13**.

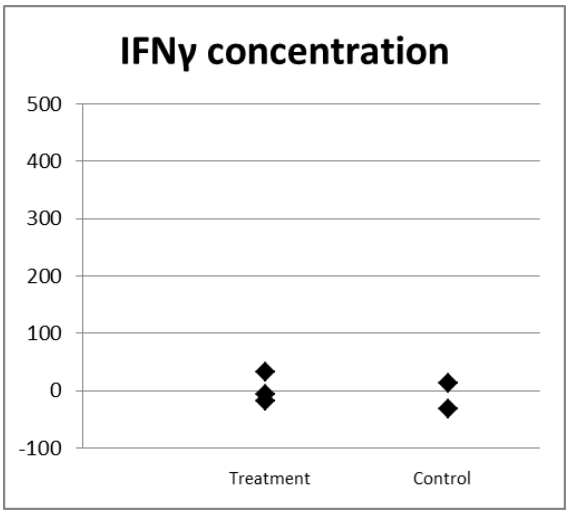

Figure 13. IFN-γ concentration measured in the serum of treated and untreated mice.

The concentration seen in both the treated and untreated mice were negligible compared to the standard curve concentrations (30-1000 pg/mL). This indicated that the injected nanoparticles did not produce a IFN-γ detectable immune response 6h post injection. In order to confirm this, an experiment was done to compare the immunological response to the nanovaccine as compared to a complete solution containing microbial peptides and soluble α-GalCer. Eight wild-type C57BL/6 mice were used for this study in four groups. Each mouse was injected intraperitoneal with 100 μL of solution based on groups. The first group, two mice, received 0.5 mg/mL SPIO nanoparticles conjugated to MUC1 peptide and α-GalCer lyposaccaride (SPIO-(MUC1, α-GalCer)). The second group received 0.5 mg/mL SPIO nanoparticles conjugated to α-GalCer (SPIO-(α-GalCer)). The third group was injected with a solution

containing MUC1 peptide (50 μg), two microbial peptides (70 μg) and α-GalCer (1 μg) (Complete). The final group was injected with two microbial peptides (70 μg) and α-GalCer (1 μg) (Mock). After 6 hours, blood was collected from each mouse. The serum was isolated with centrifuge and an ELISA was done for IFN-γ as described above. Data is reported in **Figure 14**.

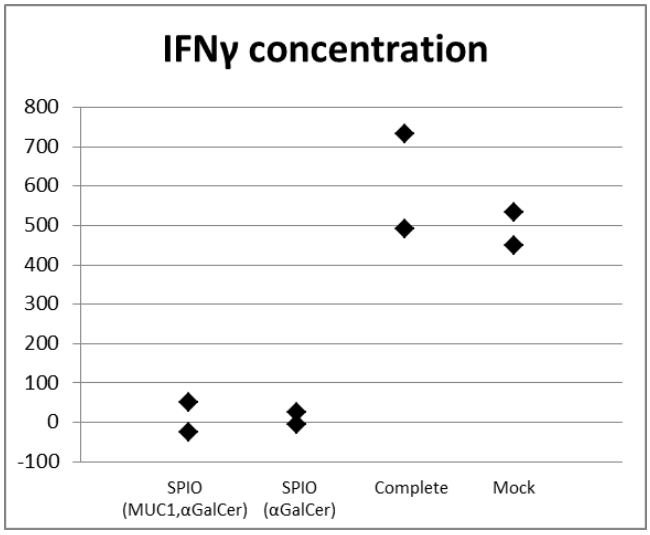

Figure 14. IFN-γ concentration measurements for each mouse are shown categorized by group.

It can clearly be seen that the synthesized nanovaccine did not activate an immune response as was expected. The positive control of soluble antigen and adjuvant with microbial peptides indicates that these molecules are capable of activating an IFN-γ producing immune response. Results of SPIO-(α-GalCer) from this study do not agree with the earlier study of nanoparticle concentration. A few caveats need to be examined. This *in vivo* analysis of cytokines may indicate that there were inconsistencies with the synthesis or conjugation of the ligands onto the SPIO nanoparticles. Particularly, amination of the nanoparticles with the epoxy amine linker is complicated, and thus

process requires skillful maneuvers. And if this foundation is not achieved reproducibly it may affect in our attempt to conjugate antigens and adjuvants. It is also noteworthy that this data represents the outcome obtained from experiments using a single set of nanovaccine compounds; more experiments need to be achieved with modifications in order to improve the therapy. For example, analytical techniques need to be performed to ensure antigens and other ligands are attached on the SPIO nanoparticles. Additionally, precise concentration of the antigen and adjuvant need to be taken in account and calibrated against the controls for *in vivo* therapy.

Alternative Approach to Aminated SPIO Nanoparticle Synthesis

In an attempt to improve the synthesis, an alternative approach for developing aminated SPIO nanoparticles was employed, modifying dextran. Dextran is a white solid and the presence of an amino group can quickly be characterized through ninhydrin staining by purple product formed (the brown color of SPIO nanoparticles prevents this test from being used to characterize the aminated product). A two-step synthesis was carried out following the procedure outlined in Rebizak et al and shown in **Figure 15** (Rebizak et al., 1997).

Step one synthesis of carboxymethyldextran (CMD) was done as follows: dextran 10 (GE Healthcare) (10.0 g, 52.0 mmol glucose units) and 6 N NaOH (82.5 mL) at room temperature were added to a 250 mL round bottom flask. Solution was stirred until dextran was dissolved. Chloroacetic acid (20.5 g, 217 mmol) was added to the solution. The mixture was stirred at 60 °C for 50 minutes then cooled to room temperature. The solution was then added to MeOH (500 mL) to producing a white precipitate. The

precipitate was filtered and washed with MeOH then dried under high vacuum producing a white solid, CMD (9.119 g, 65.7% yield).

The second step proceeded as follows: To a 250 mL round bottom flask containing 100 mL of H_2O was added CMD (10.0 g, 36.7 mmol glucose units). The solution was stirred until the solid had dissolved then the pH was adjusted to 3 using 1N HCl. A 2-Ethoxy-1-(ethoxycarbonyl)-1,2-dihydroquinoline (EEDQ) solution was prepared as follows: EEDQ (15.4 g, 62 mmol) was added to a 250 mL round bottom flask containing MeOH (233mL). The EEDQ solution was added drop wise to the CMD solution with stirring to avoid formation of a precipitate. Ethylenediamine (20.7 mL, 310 mmol) was added to the solution and left at room temperature for 4 hours. The solution was then added to MeOH (500 mL) producing a white precipitate. The precipitate was filtered and washed with MeOH then dried under high vacuum producing a white solid, aminated carboxymethyldextran (CMDA) (7.840 g, 73.3% yield).

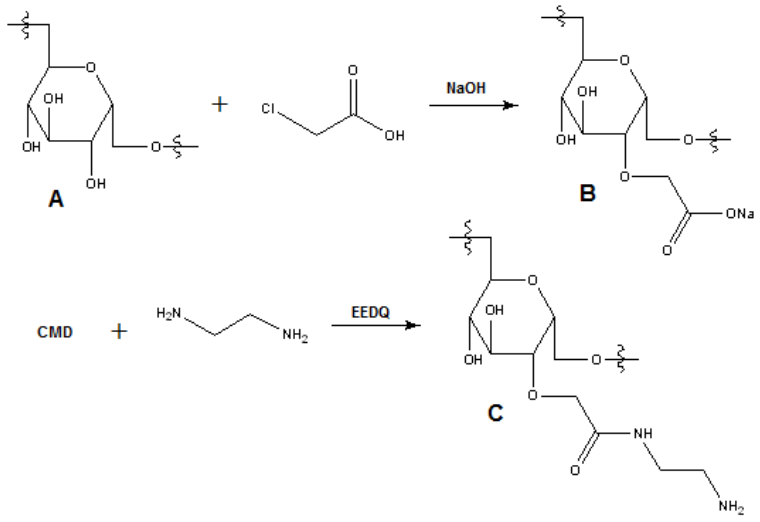

Figure 15. Scheme of CMDA synthesis. Dextran (A) is converted to a carboxylic acid in CMD (B) and further conjugated to an amine terminus in CMDA (C).

A portion of the CMDA product, CMD, and dextran were dissolved in water and spotted on a TLC plate. After drying, ninhydrin (2,2-Dihydroxyindane-1,3-dione) solution was added and the plate was heated on a hot plate at 80 °C for approximately 5 minutes. The CMDA spot appeared purple, while the CMD and dextran spots did not color. Although ninhydrin test of the product were positive for the amino group, ^{1}H NMR of the polymer did not show consistent results (data not shown). ^{13}C NMR was also unable to verify the synthesis of the CMDA product. Final characterization was done with Fourier transfer-Infrared (FT-IR) spectroscopy to show the appearance of an amine peak as compared to the Dextran. All samples were prepared by placing 20 μL of solution (50mg/ml) on Germanium Attenuated Total Reflection (Ge ATR) crystal to form a film (~ 1 cm diameter).

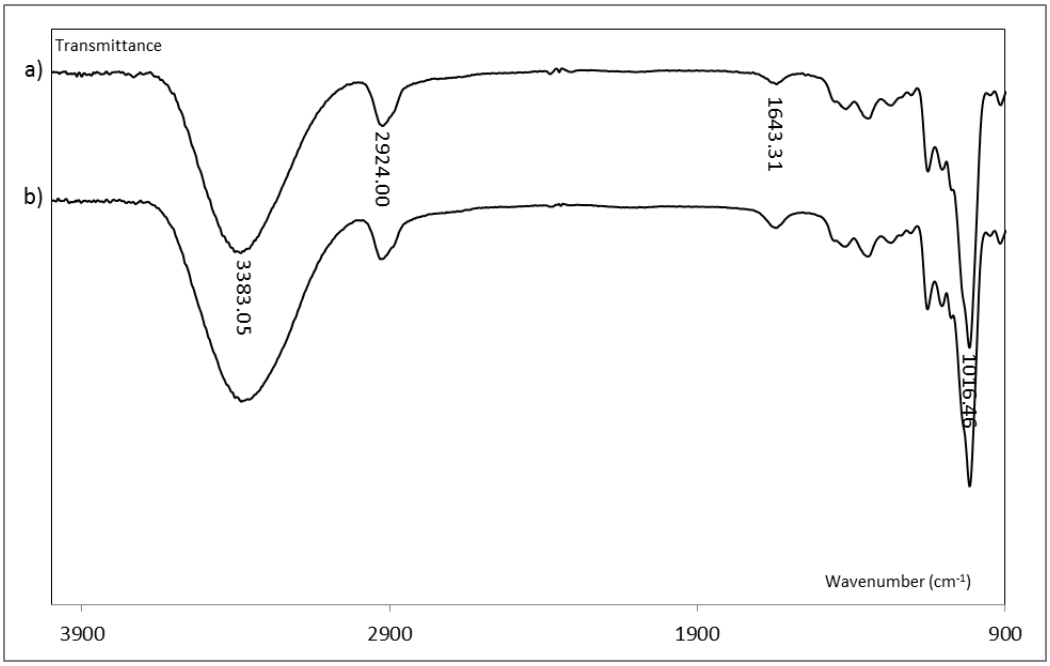

Figure 16. FT-IR of Dextran (a) versus the CMDA product (b). A new amino group would show a peak around 1650 cm^{-1}.

The FT-IR was expected to show a deep increase in the peak near 1650 cm^{-1}. As can be seen in **Figure 16** only a negligible difference can be seen between the CMDA product and dextran starting material around 1650 cm^{-1}. The negative results seen here were supported by failure to achieve coating of SPIO nanoparticles comparably to dextran.

Future Work

Further work is being done in this area to improve synthesis of the nanoparticle. Alternate synthesis of an aminated coating material is being developed. With improvement of the aminated nanoparticle the conjugation to MUC1 peptide and α-GalCer can be analyzed and adjustments made to optimize the number of biomolecules

on the surface of the nanovaccine. Combination of antigen and adjuvant to the surface of the nanoparticle is expected to induce a powerful immune response. To verify this, studies can be done *in vitro* to assess production of cytokines when pulsed to immature DCs. Movement into *in vivo* studies will analyze the immune response to the nanovaccine as previously described through concentration measurements of cytokines such as IL-4 and IFN-γ, including analysis of the mechanism of immune activation. These measurements can be done with a variety of injections routes to find the optimal means of creating an immune response. Although inconclusive, preliminary data of a positive tumor response to the nanovaccine is observed. Tumor response studies in murine models should be repeated to verify this finding and optimize treatment. Treatment with the nanovaccine alone should be compared to treatment with nanovaccine pulsed DCs to verify that the nanovaccine alone is able to activate immune response comparable to the standard procedure at this time.

CHAPTER III

Nebulization

Rationale

Immunotherapy has been developed from varied angels of attack, which has led to inconsistencies between research groups in the best means of attaining an immune response. One area in which this is apparent is the route of delivery. Attention has be drawn to the fact that no consensus has been reached on the best way to reintroduce pulsed DCs into the patient (Pham et al., 2009). This step is of importance due to the requirement that the mature DCs are able to migrate to the LN and present the antigen to the T cells. A study done as late as 2011 (Bouvier et al., 2011) continued to examine the route of delivery, directly testing two of the possible routes against each other, intradermal and intravenous injection. Each route was found to have advantages over the other and again a consensus could not be reached as to the best route of delivery across the board.

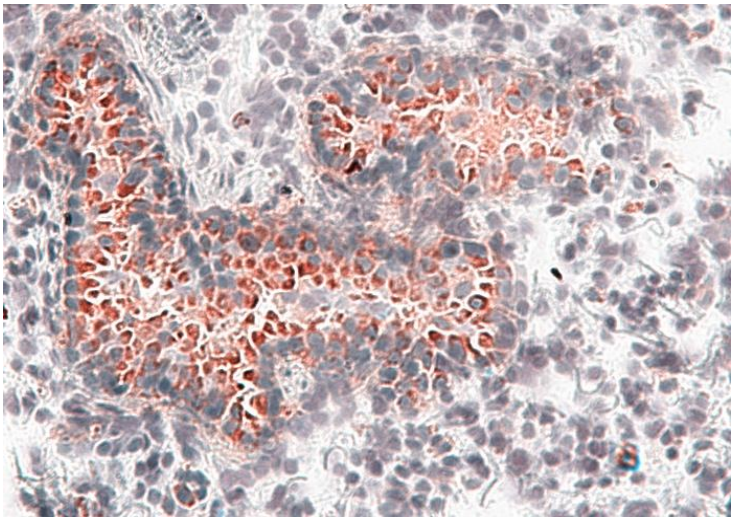

Figure 17. CD11c staining in lung tissue shows the presence of DCs.

The development of a nanoparticle delivery system containing antigen and adjuvant molecules allows for the possibility of DC uptake of the nanovaccine *in vivo*. In this case the route of delivery must be analyzed separately from the traditional immunotherapy approach. Areas rich in endogenous DCs are optimal for delivery of the nanovaccine allowing for the greatest chance of DC uptake. DCs are widely distributed in the body, although they comprise only a small proportion (0.1-1%) of the cells in different lymphoid and non-lymphoid tissues (Ema, 1990). Sertl et al studied histology of the lung to determine that the epithelial cells contained 1% DCs, which were found to be powerful APCs. The DCs were the only MHC class II antigen-positive cells found in the tracheobronchial epithelium. They were present in the epithelial cells extending toward the lumina, in the vascular walls, and were found peripherally as far as the alveolar septa and the visceral pleura (Sertl et al., 1986). Lung tissue contains some of the highest concentration of DCs because DCs on the epithelial surfaces, including the lungs, play a vital role in the induction of both innate and adaptive immunity. A need to

maintain local homeostasis, as well as, exposure to airborne antigens requires fine control of immunological processes (Holt et al., 1993). Signals for the adaptive immune response come from a variety of stimuli in the lungs; allergens, environmental pollution, microorganisms within the respiratory tract, and innate immune cells must be processed as signals for the T cells (Lambrecht and Hammad, 2010). "The large surface area, extensive vascularization and thin epithelium in the alveolar lung tissue might facilitate efficient systemic delivery of antigens (Sou et al., 2011)." The action of DCs as well as intrinsic qualities of the lung tissue provides a prime target for *in vivo* immunotherapy.

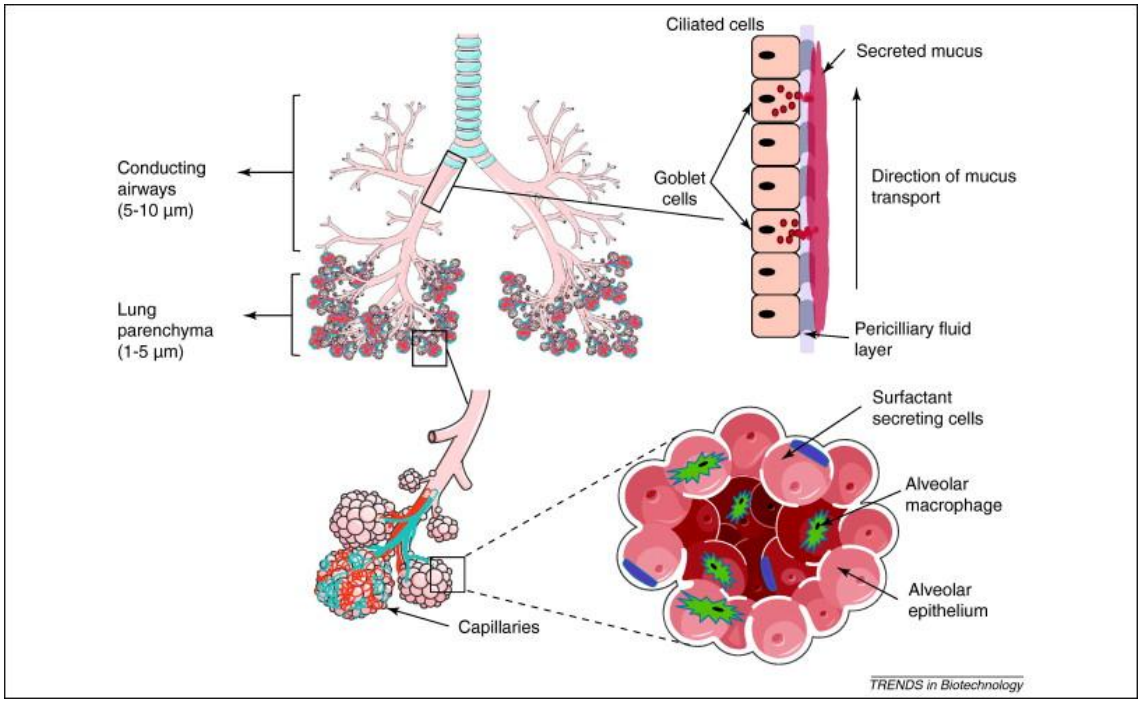

Figure 18. Diagram of the lung and particle-size requirements based on intended deposition region in the respiratory tract. Images on the right are magnified, cartoon views of tissue structures of the conducting airways (i.e. trachea, bronchi and bronchioles) and alveoli in the parenchyma region. Immunosuppressive alveolar macrophages and serum-derived antibodies provide a final line of protection against invading pathogens. A cellular and humoral immune response can be generated after interaction with innate immune receptors present on epithelial cells and tissue-resident DCs. (Sou et al., 2011)

The development of a nanoparticle delivery system for cancer immunotherapy circumvents the need for isolation of the DCs from the patient, as well as, the adaptive transfer of pulsed DCs back into the patient. Pulmonary delivery of nanoparticles has been shown to promote antigen uptake and trafficking to the draining LN by intrinsic DCs (Nembrini et al., 2011). The delivery of tumor vaccines in form of an aerosol offers several advantages over the current distribution methods. First, the technique does not require DC isolation. Second, *in vivo* activation of endogenous DCs will bypass uncertainties associated with isolating DCs *ex vivo*, DC activation, and reimplantating of DCs. Third, a future combination of aerosol delivery, targeted release of tumor antigens inside residential lung DCs, and imaging will allow for an unprecedented level of simplicity and reliability with the added benefit of a monitored response. A study in 2011 (Nembrini et al., 2011) found that when Pluronic-stabilized poly(propylene sulfide) (PPS) nanoparticles were delivered to the lungs, there was no visible change in lung morphology and no sign of permanent inflammation. The study indicates that pulmonary administration of nanoparticles is not harmful to the lungs. In this work, we attempt to validate delivery of aerosolized nanoparticles into the lungs of mice and track the migration of particle-laden DC's into the draining LNs.

Methods and Results

Nasal Nebulization

Nebulization of 30 nm SPIO nanoparticles conjugated to the epoxy amine linker was achieved using the Aeroneb Lab Micropump Nebulizer (Aerogen, Danagan, Ireland)

rated to produce an aerosol with particles of 2.5-4.0 µm mean diameter. Two mice were nebulized in the provided mouse holding tube with 5 mL of SPIO nanoparticles twice at approximately a 3 hour interval. The mice were sacrificed 24 hours post nebulization and the lungs isolated and frozen for histological staining. The efficiency of SPIO nanoparticle delivery was confirmed with Prussian blue staining. 8 µm frozen sections of the harvested tissue were immobilized on a glass slide. The slides were dried at room temperature and fixed with 4% paraformaldehyde for 5 minutes. The samples were then stained with a freshly mixed 2.5% hydrochloric acid and 2.5% potassium ferrocyanide solution for 30 minutes. After washing with water, the slides were counterstained with 0.1% nuclear fast red for 10 minutes. The slides were then visualized with light microscopy using a Zeiss Axioskip 40 microscope (Carl Zeiss MicroImaging, Thornwood, NY) equipped with AxioCam (Carl Zeiss MicroImaging, Thornwood, NY) for digital images with a 40 objective lens.

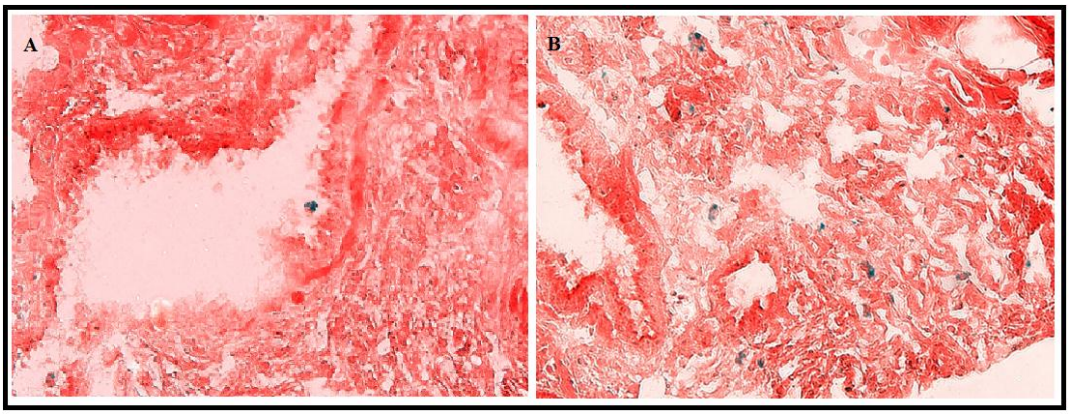

Figure 19. Prussian blue staining of representative slides from two nebulized mice.

Figure 19 shows one representative slides from each of the mice that were nebulized with SPIO nanoparticles, although the nanoparticles can be detected in the lungs of these mice, the amount that is delivered is very small and improvements to nebulization techniques used in these mice are needed to more accurately mimic clinical nebulization.

Nebulization through Intubation

In order to improve the delivery of SPIO nanoparticles to the lungs of mice through nebulization, the nebulization was directed to the lungs through intubation, bypassing the instinct of the mouse to avoid inhaling the vapor. Mice were anesthetized with an intraperitoneal injection of 0.06 mg/g ketamine and 0.01 mg/g xyalizine mixture. The animal was suspended from its front incisors. A 20 gauge Surflash polyurethane intravenous catheter and needle (Terumo, Somerset, NJ) were selected. The 20 gauge needle was discarded. A flexible fiber optic stylet was connected to a light source (Kent Scientific, Torrington, CT) and was attached to the catheter. Under direct visualization, the stylet-catheter system was placed through the larynx and into the trachea of the animal. The stylet was subsequently removed. Placement of the endotracheal tube was verified by occluding the tube with a drop of water and observing for movement with animal respiration. After confirming correct placement, the drop of water was removed and the endotracheal tube was connected to the ventilator and nebulizer in the configuration depicted in **Figure 20**, the mouse was placed on a heating pad while under anesthesia during nebulization.

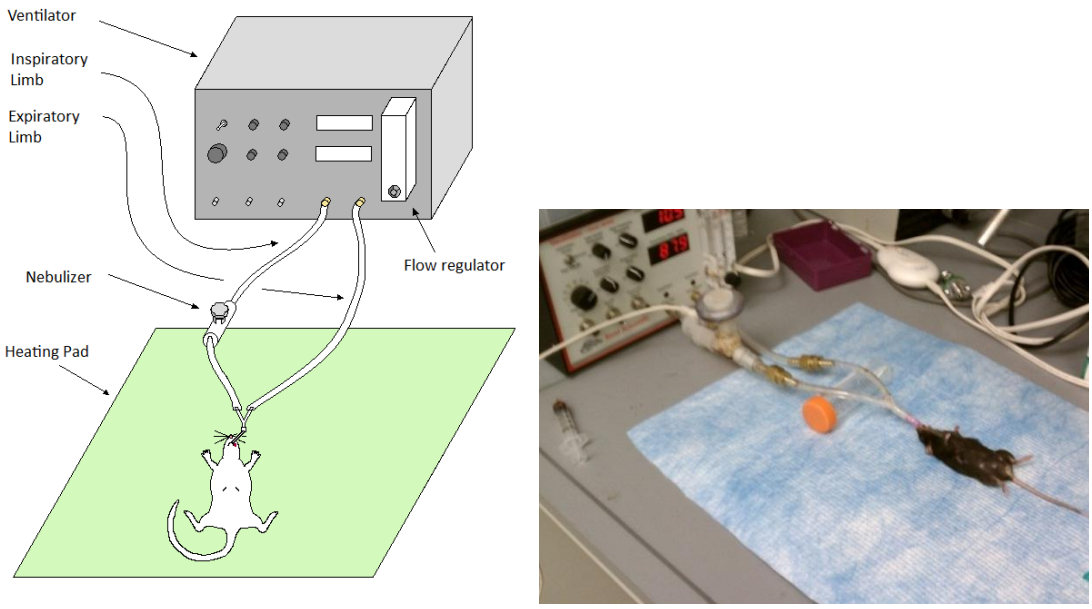

Figure 20. A scematic of the nebulization through intubation system used is shown on the left next to a picture of the system in use on the right.

The mouse was ventilated with a Topo Dual Mode Ventilator (Kent Scientific, Torrington, CT) supplying 120-150 breaths per minute, a peak inspiratory pressure between 10-15 cm H_20, and an airflow of approximately 3 L per minute, using an Aeroneb Lab Micropump Nebulizer (Aerogen, Danagan, Ireland). Five 1 mL aliquots of SPIO nanoparticles were passed through the nebulizer and delivered into the endotracheal tube. During ventilation and nebulization, the mouse was also monitored for signs of respiratory distress, such as abdominal contractions, which indicated that the animal was breathing against the ventilator. If distress was identified, ventilation and nebulization were paused, and the mouse was immediately extubated. After the distress resolved, the mouse was reintubated, ventilated and supplied with nebulized SPIO nanoparticles as above. The level of anesthesia was also monitored by testing the palpebral reflex and

response to tail pinch. Additional anesthesia was administered as needed to maintain the appropriate anesthetic plane.

After successfully nebulizing 5 mL of SPIO nanoparticles, the mouse was disconnected from the ventilator and extubated. Recovery from anesthesia was monitored by testing the righting reflex. The animal was sacrificed 24 hours after nebulization. The trachea, lungs, and mediastinal LNs were harvested, embedded in optimal cutting temperature compound, and frozen for subsequent histology.

Prussian blue staining to confirm the presence of SPIO nanoparticles was done as previously described in both the lung and LN tissue. Consecutive slides were stained for DCs with immunohistochemistry. The 8 μm frozen sections of the harvested tissue were immobilized on a glass slide were dried at room temperature, rehydrated with 0.1 % tween 20 in PBS, and treated with hydrogen peroxide to neutralize any endogenous peroxidases. The samples were then treated with bovine serum albumin (BSA) (Lab Vision, Fremont, CA) to block any nonspecific staining prior to primary antibody addition. After incubating the slides for 120 minutes with affinity-purified hamster anti-CD11c antibody (eBioscience, San Diego, CA) diluted 1:200 in BSA, the slides were rinsed and incubated for 1 hour with purified goat anti-hamster antibody conjugated to biotin (eBioscience, San Diego, CA) diluted 1:1000 in BSA. The slides were subsequently washed and treated with the Vectastain ABC Elite system (Vector Laboratories, Burlingame, CA) and 3,30-diaminobenzidine (Dako, Carpinteria, CA) to produce localized, visible staining. Finally, the slides were counterstained with Meyer's Hematoxylin (Sigma-Aldrich, St. Louis, MO). All sections were visualized with light microscopy as previously described.

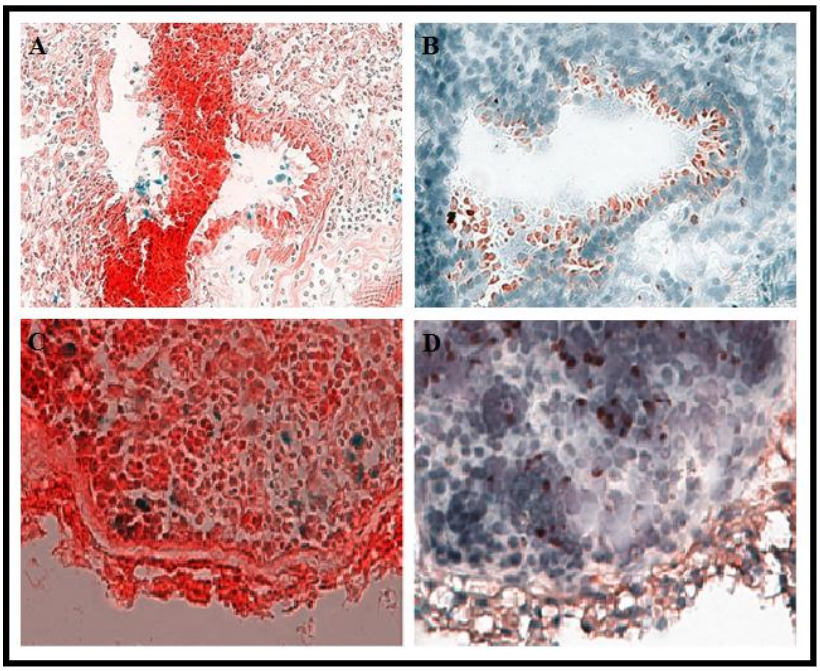

Figure 21. Prussian blue iron staining in the lung tissue (A) and LN (C) 24 hours after nebulization. CD11c immunohistochemistry for DCs of consecutive slides in the lungs (B) and LN (D).

Confirmation of the delivery of the SPIO nanoparticles to the lungs can be seen in **Figure 21**. The increase concentration of the iron compared to the previous study indicates the increased efficiency of nebulization using intubation over the nebulization alone. Consecutive slides stained with CD11c show the area rich in DCs. Co-localization of the SPIO nanoparticles and DCs in consecutive slides proves promising toward the goal of cellular uptake by the DC of our delivery molecule. Prussian blue staining within the mediastinal LN is positive for the presence of SPIO nanoparticles supporting our hypothesis of DC migration from the lungs to LN after uptake of the nanoparticles.

Nebulization with Hybrid Imaging Nanoprobe

The same nebulization techniques were used in a study using fluorescent magnetic hybrid imaging nanoprobe (HINP). The probe was a conjugation of SPIO and visible light emitting fluorescent CdTe/CdS quantum dots (QDs) developed by D. Koktysh (Koktysh et al., 2011). The multimodal imaging agent combines an ability to be visualized by magnetic resonance (MR) imaging and through optical imaging. This opportunity for optical imaging was used to verify the data obtained from the previous nebulization experiment. The nebulization was performed as previously described after sedation with intubation. In this experiment 10 mg/mL samples of HINP were diluted to 4 mL in PBS. The mouse received 2 mL of this solution through nebulization. Imaging of the distribution through the whole mouse was not possible due to the thick and pigmented skin of the black mouse (C57BL/6). After approximately 5 hours the mouse was sacrificed and the lung and mediastinal LN were isolated for *ex vivo* imaging shown in **Figure 22**.

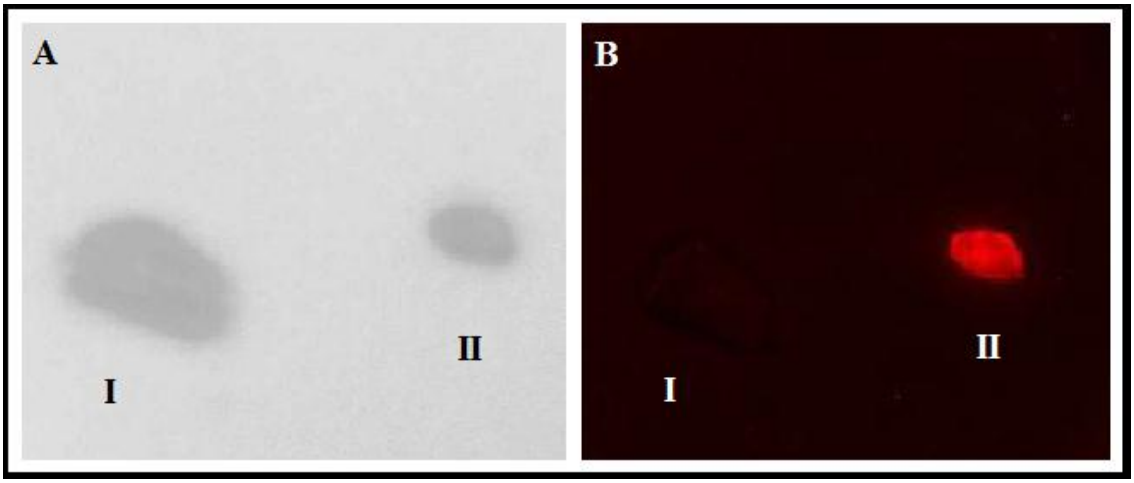

Figure 22. White light (A) and fluorescent (B) images of muscle tissue (I) compared to a dissected draining LN (II) of a mouse 24 hours post treatment. (Koktysh et al., 2011)

The HINPs were able to be visualized in the lungs (data not shown) and in the mediastinal LN (**Figure 22**). The results showing migration of the nanoparticles to the draining LN is promising for the future of immunotherapy using SPIO nanoparticles as a delivery vehicle to the endogenous DCs of the lungs.

Future Work

Due to problems with safety of intubated mice and inconsistencies between mice, in the future the work will move to use a new nebulization system seen in **Figure 23**. This custom designed nebulization system has advantages over previous systems. The system allows for nebulization of three mice simultaneously, providing consistency across multiple mice (**Figure 24**). The system includes an automated plunger which provides a constant flow of an inhalable amount of aerosol as opposed to nebulizing with multiple aliquots. Nebulization occurs through a Jet nebulizer which works by passing the liquid to be aerosolized across a high pressured stream of air. Unlike the mircopump

nebulizer this allows for constant production of aerosol at a slower, manageable rate. The excess solution, that which is not aerosolized after passing through the stream of air, can be collected and quantified to determine experimental dose.

Figure 23. Nebulization system in which three mice may be nebulized simultaneously, therefore in more closely related conditions.

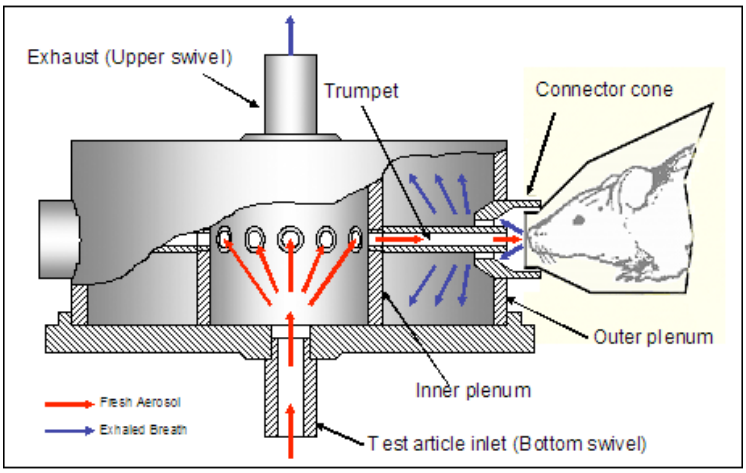

Figure 24. Diagram of multi animal nebulization system indicating the route the aerosol takes during delivery to mice.

With verification of the advantages of the new nebulization system over previous nebulization techniques and the completion of a well-defined antigen/adjuvant conjugated SPIO nanoparticle, progress can be made toward utilizing the information of nebulization to properly deliver immune activating molecules to the resident DCs in the lungs. This delivery can then be compared to delivery through injection and pulsed-DC through cytokine concentration studies and tumor response studies. Comparable treatment response with nebulization to other more difficult techniques will verify the use of aerosol delivery for immunotherapy and provide a simplified route of vaccinating against cancer.

CHAPTER IV

Near Infrared Dye

Rationale

Optical imaging is a powerful tool for non-invasive mapping of molecular events. Unlike other imaging modalities, optical imaging does not require contact with any iodizing radiation and is cost efficient. Optical imaging involves detection of electromagnetic waves within the visible, infrared, and ultraviolet wavelengths. Emission of these wavelengths from the studied source can be produced in two ways, fluorescence and bioluminescence. Bioluminescence is release of light due to chemical reactions occurring intrinsically in an organism. This may be added to cells through transfection of bioluminescent genes. Fluorescence occurs when a chromophore absorbs light and is excited to a higher energy level. The molecule then relaxes and omits fluorescent light. Fluorescent molecules have been conjugated to certain molecules in order to target a specific molecule or process *in vivo*. A variety of targeting molecules can be used for a multitude of purposes including small-molecules looking at the folate receptor, peptides to image fibrin, proteins to study angiogenesis, and antibodies for the HER2/neu marker of cancer to name a few (Hilderbrand and Weissleder, 2010). An ideal fluorescent dye for labeling of biomolecules must be water-soluble and chemically stable; it should have a large fluorescence quantum yield. Inclusion of a reactive functional group which is stable in storage but has specific, highly efficient labeling to the targeting molecule producing a stable covalent bond is also important (Flanagan et al., 1997).

NIR dyes are of particular interest in optical imaging due to the low *in vivo* absorbance in these wavelengths. Biological chromophores are strong absorbers of visible light whereas other biomolecules absorb in the infrared. The optimal imaging window is between 600 and 1000 nm, NIR (Hilderbrand and Weissleder, 2010). Limited absorbance in this range allows for imaging to a depth of a few cm rather than the 1-2 mm limit of visible wavelength fluorophores (Ntziachristos et al., 2003). As wavelength increases, scattering and autofluorescence decrease lowering the background and therefore greater contrast (Pham et al., 2008). NIR emitting molecules are either small molecule dyes or nanoparticles. Nanoparticle distribution is favorable due to its longer blood half-life, but small molecule dyes are powerful due to the ability to design molecules with large Stokes shift (the distance between absorbance and emission peaks) (Hilderbrand and Weissleder, 2010). Two families of fluorescent dyes are cyanines and rhodamines. Cyanines basic structure is a conjugated methionine bridge connecting two nitrogen-containing heterocyclic rings (Nolting et al, 2012). Absorption and emission of cyanine dyes are dependent on their structure and can be designed based on known parameters. The length of the polymethine chain and the identity of the heterocyclic rings effects on the overall absorption and emission wavelengths have been well characterized and can be tuned to the NIR region while keeping a compact structure compared to other dyes (Pham et al., 2005). Rhodamine dyes are identified by conjugated hexagonal heterocycle backbone based off a xanthylium. They usually contain a site that can be used for bioconjugation and are therefore popular for labeling of biomolecules (Nolting et al, 2012).

IR-783 (see **Figure 25**) is a commercially available cyanine dye with absorbance and emission in the NIR range. The 7-carbon length methionine bridge between indole rings determines the absorbance of this dye, with maximum between 779 and 785 nm. This stable dye is water soluble due to the addition of sulfonic acids. The methionine bridge is stabilized by incorporation of the center three carbons into a 6-member ring.

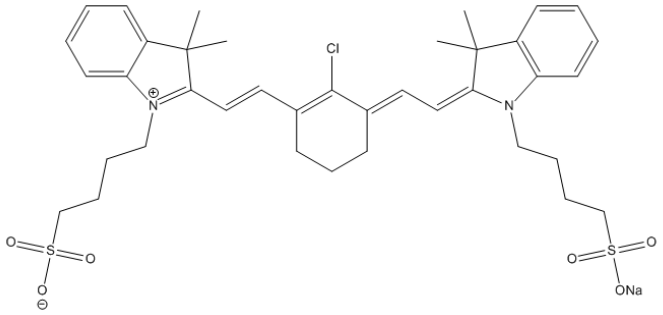

Figure 25. Structure of commercial NIR dye, IR-783

The commercial dye is ideal for optical imaging due its stability, water solubility, and NIR absorbance and emission, but lacks a site for bioconjugation. Through chemical modification at the halide group a bioconjugation site can be added without interrupting the other necessary characteristics of this NIR dye for targeted imaging.

Methods and Results

Functionalization of Dye

The commercial dye, IR-783, is limited in its use as an optical probe by the absence of a site for bioconjugation to targeting molecules. Pham et al. describes a

reaction whereby a halide containing cyanine dye can be modified to contain a carboxylic functional group (Pham et al., 2008). The nucleophilic substitution by aminoundecanoic acid of the Cl improves the dye as a targeted optical probe in two ways: the inclusion of the carboxylic acid bioconjugation site and an increase of stokes shift from 30 nm to 140 nm. The same reaction can be applied to IR-783 in order to prime the molecule for labeling activation, generating a product that can readily be modified to a reactive compound, such as a succinimidyl ester.

Synthesis, as seen in **Figure 26**, was performed as follows: IR-783 (50.4 mg, 67.3 mmol), 11-aminoundecanoic acid (17.9 mg, 88.9 mmol), and ethanol (EtOH) (4 mL) were added to a 2-5 mL microwave reaction vial (Biotage, Charlotte, NC). A stirbar was added and the vessel was sealed. The solution was reacted in the microwave "Initiator" (Biotage, Charlotte, NC) for 1 hour at 100 °C with 30 seconds pre-stirring. The product was verified by the appearance of a blue spot on TLC done in 2.5/7.5 MeOH/ dichloromethane (DCM). The solution was loaded on a silica gel column for use on CombiFlash (Teledyne ISCO, Lincoln, NE) and purified using a 40 g column. The fractions corresponding to the blue TLC spot were collected and dried. The blue solid intermediate (B) was formed (32.4 mg, 65% yield).

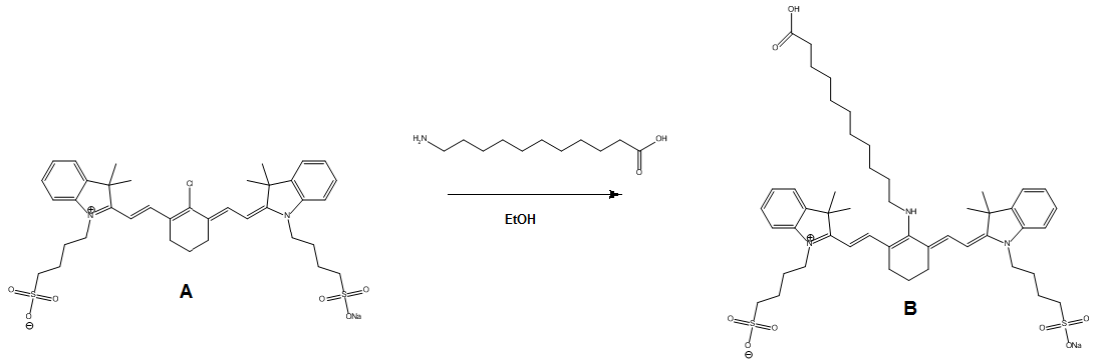

Figure 26. Scheme for functionalization of NIR dye.

The reaction was monitored by a color change in the reaction solution, specifically from green to blue. Absorbance and emissions spectra of the starting material (IR-783) was compared to the new blue intermediate, obtained from UV-vis Spectrophotometer (Agilent Technologies, Santa Clara, CA) and Fluorimeter (Photon Technology International, Birmingham, NJ) The resulting excitation/emission peaks are graphed in **Figure 27**.

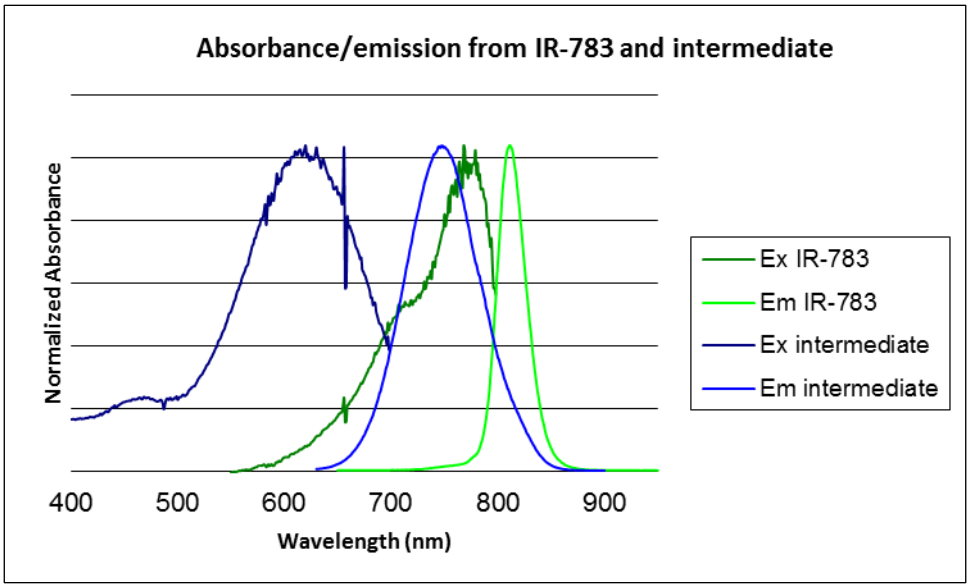

Figure 27. Absorbance and emission spectra from IR-783 and the blue intermediate normalized to maxima.

The addition of 11-aminoundecanoic acid in place of the Cl atom shifts the excitation maximum from 780 nm to 610 nm. The shift of emission maximum is small from 810 nm to 750 nm. An increase of Stokes shift from 30 nm to 140 nm widens the number of applications this dye may be used for, especially making the new dye ideal for such application as FRET.

Activation for Biomolecule Conjugation

There are a variety of molecules which can be used to activate a dye for bioconjugation; one of these is addition of a succinimidyl ester moiety (Flanagan et al., 1997). Succinimidyl ester is ideal because of it specific reactivity to primary amines present, including peptides and proteins, to form a stable peptide bond (Banks and Paquette, 1995).

The second step of activating the NIR dye is as follows (**Figure 28**): the dye intermediate (B) (32.4 mg, 35.4 mmol), N,N'-dicyclohexylcarbodiimide (DCC) (12.6 mg, 61.1 mmol), and NHS (12.9 mg, 112.1 mmol) were added to a dry 10 mL round bottom flask. The flask was then purged with nitrogen and placed in a 0 °C ice bath. DMF (2 mL) was added to the flask to dissolve the solids. The reaction vessel was allowed to warm to room temperature for 5 days until a precipitate, dicyclourea byproduct, was formed. The solution was filtered and the filtrate was collected. A TLC was done in 2.5/7.5 MeOH/DCM showing separation of product from intermediate (B). The solution was loaded on a silica gel column for use on CombiFlash (Teledyne ISCO, Lincoln, NE) and purified using a 40 g column. The fractions corresponding to the product TLC spot were collected and dried. A portion of dry product was sent to Mass Spectrometry Core for analysis by Time of Flight (TOF) Mass Spectrometry (MS) (**Figure 29**).

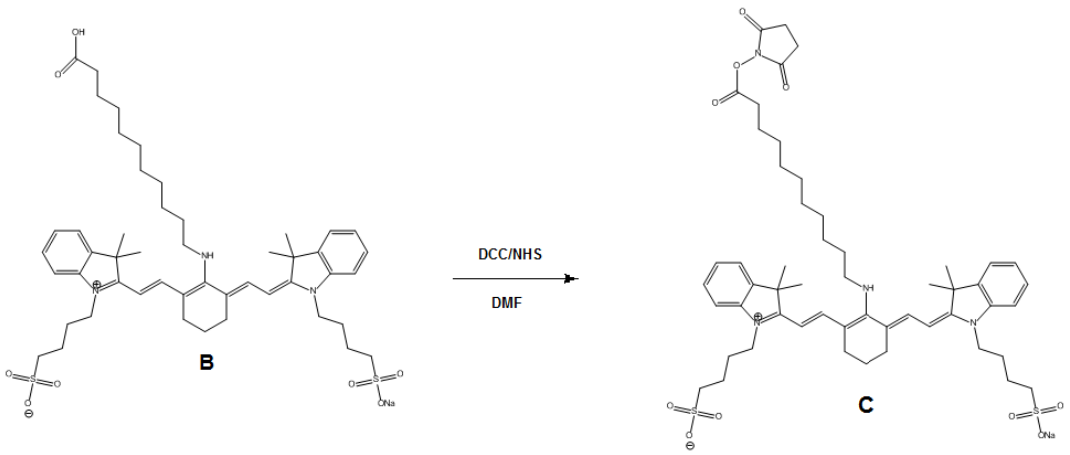

Figure 28. Scheme for activation of NIR dye.

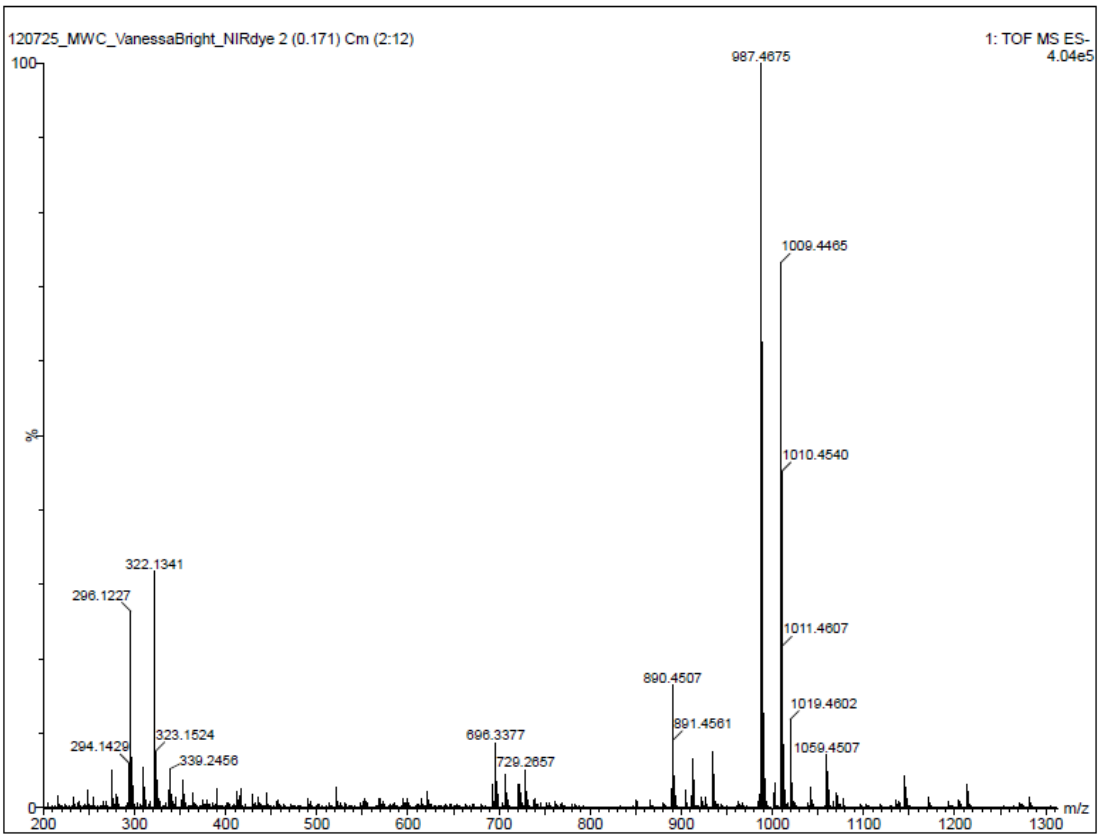

Figure 29. MS data shows the presence of the activated NIR dye product (m/z 987.4675) with a small amount of starting material (m/z 696.3377) and intermediate (B) (m/z 890.4507) impurities.

MS indicates that the bioconjugation activated NIR dye was produced, with small amounts of precursor impurity. The excitation and emission spectra of the final product was determined as previously described.

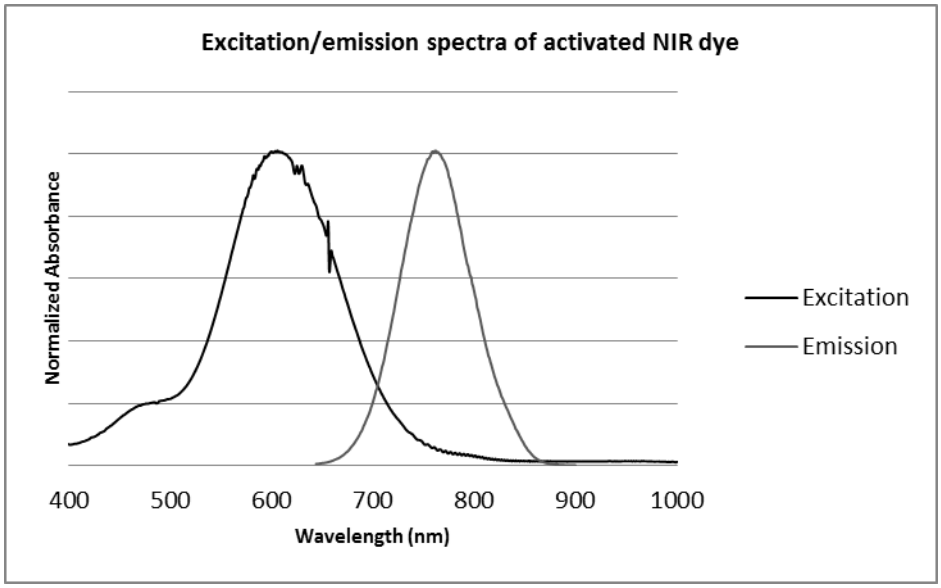

Figure 30. Excitation and emission of succinimidyl ester activated NIR dye product.

Figure 30 show the succinimidyl ester activated NIR dye retains the fluorescent properties of the reaction intermediate that are seen in **Figure 27**. This includes a large Stokes shift of approximately 150 nm.

Labeling Study

To validate the bioconjugation ability of the succinimidyl ester NIR dye product a protein of interest was chosen. Peanut agglutinin (PNA) is a protein which has been used to target imaging probes, both optical and radiolabeled, for mammary cancer cells (Seitz et al., 1984); (Shysh et al., 1985). PNA is known for its high affinity binding to the Thomsen-Friedenreich antigen (TF-antigen). TF-antigen is a known marker for adenocarcinoma cells of the breast (Seitz et al., 1984). Labeling of this protein for optical imaging will allow increased observance of the tumor cells during therapy, increasing the ability to characterize the action of the SPIO nanovaccine.

Biotinylated PNA (5 mg) and activated NIR dye (1.1 mg) was placed in a 10 mL round bottom flask. PBS (1.5 mL, pH 7.49) was added and the solids dissolved. The reaction was left under nitrogen for 4 hours. The product was purified with a PD-10 desalting column (GE Healthcare, Pittsburgh, PA) according to the manufacturer's instructions with PBS. The first blue band to pass through the column was collected. Absorbance spectra were determined with UV-vis Spectrophotometer (Agilent Technologies, Santa Clara, CA) of NIR dye before addition of the PNA and after the reaction. The appearance of a peak between 260 and 280 nm (from the reaction byproduct, NHS) indicates success of the reaction (**Figure 31)**. To confirm the absorbance was due to NHS, the absorbance was measured again after passing through the desalting column.

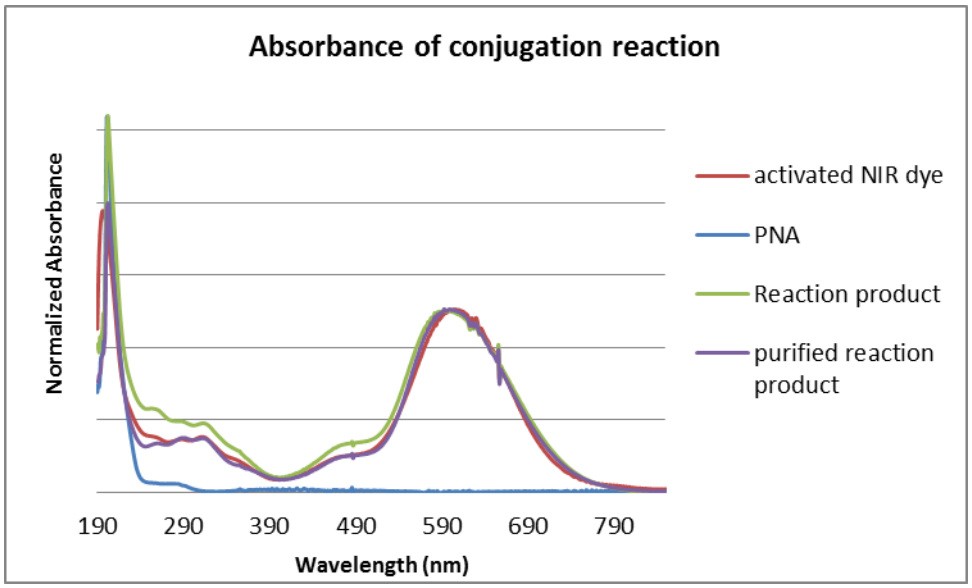

Figure 31. Absorbance of activation reagents and product normalized to dye peak. Increase in absorbance between 260-280 nm indicates formation of the byproduct, not seen after purification.

Future Work

The PNA targeted NIR dye can be used in the future to visualize the breast cancer tumors in the *in vivo* studies of treatment response, providing another means of gaining information about the efficacy of the nanovaccine. The shape and size of the tumor can be more accurately measured using optical imaging and the PNA conjugated NIR dye.

The labeling of PNA shows that the modified commercial dye, IR-783, is a powerful tool for optical imaging in the NIR region. The addition of the functional group and activation with a succinimidyl ester is a relatively simple synthesis that can be readily repeated. Addition of the succinimidyl ester allows for bioconjugation to a number of biomolecules. Further work can be done with this dye in a variety of studies through conjugation to any number of targeting molecules containing an amino group.

CHAPTER V

Discussion

This thesis describes our work in immunotherapy, the use of SPIO nanoparticles as delivery molecules and for imaging, and our synthesis of a bioconjugatable NIR dye. The continued prevalence of cancer validates the need for the work we are doing in cancer therapy and imaging. Specifically, the discovery of DCs and the development of DC-based immunotherapy show promise as an approach to treating cancer. Pre-clinical and clinical model studies have demonstrated the efficacy of immunotherapy despite the fact that this method is not without problems (Flamand et al., 1994; Grabbe et al., 1991, Mayordomo et al., 1995; Porgador et al., 1996; Hsu et al., 1996; Thurner et al., 1999; Fong et al., 2001; Lodge et al., 2000; Nair et al., 2002; Sadanaga et al., 2001; Brossart et al., 2000; Holtl et al., 1999; Kugler et al., 2000). Nevertheless, advances can be made in this area of research in order to achieve ultimately favorable outcomes for cancer patients. The chemical probes discussed in this thesis can be classified as molecular imaging probes. The development of such probes for molecular imaging is a vital new element not only in cancer detection, but also in monitoring biological processes, drug discovery and development initiatives.

The use of SPIO nanoparticles as delivery molecules enables the conjugation of multiple molecules to the same nanovaccine as well as increase uptake in DCs compared to small antigen peptides alone (Hirosue et al., 2010). The use of MUC1 for immunotherapy has been well defined and therefore represents an ideal antigen with

which to test a new therapy technique (Kobukai et al., 2011). In that process, difficulties were experienced in the anime coupling to SPIO nanoparticles as well as the conjugation to biomolecules. The epoxy amine linker was developed from sensitive chemistry to ensure the ready availability of epoxide for nanoparticle coupling. Thus, the process requires highly skilled chemists to perform the task. Unfortunately, the absence of a simple procedure with which to verify epoxy amine coupling to the SPIO nanoparticles adds to the uncertainty regarding the consistent production of aminated SPIO nanoparticles. Attempts were made to circumvent this by producing a previously aminated CMDA dextran by following a published procedure. The success of that molecule would be a landmark development since it would facilitate straightforward verification through ninhydrin staining, a technique that cannot be used on aminated nanoparticles due to its brown color. While ninhydrin staining of the CMDA product indicated the presence of a primary amine, NMR results did not support that finding. Final FT-IR spectroscopy of the product indicated no amine frequency peak, and FT-IR data was supported by the inability to coat the SPIO nanoparticles. Ultimately, this synthesis approach was abandoned as a possible alternative to the epoxy amine linker.

Regarding the immunotherapy, we demonstrated as evidence that α-GalCer is a powerful adjuvant for activation of the innate immune system by modulating the production of IL-4 in **Figure 10**. The α-GalCer works through a variety of pathways to activate the immune response. Importantly, the conjugation of α-GalCer to SPIO nanoparticles does not inhibit that function.

Conjugation of MUC1 and α-GalCer to SPIO nanoparticles was accomplished using the same approach as α-GalCer alone; yet the results derived via this nanovaccine

disagree with those of α-GalCer alone. The concentration of conjugated biomolecules could be calculated by the release of the by-product pyridine-2-thione. Conjugation to SPIO nanoparticles was limited for both biomolecules. We observed 2.6% of the available MUC1 and 8.7% of the α-GalCer was conjugated to the SPIO nanoparticles. Modification of the procedure by increasing the incubation time of SPIO nanoparticles with SPDP failed to improve conjugation to SPIO nanoparticles. The possibility exists that the absorbance of SPIO nanoparticles alone could mask the detection of pyridine-2-thione at 343 nm, but therapy results and cytokine production support the conclusion that conjugation to the SPIO nanoparticles was not as successful as expected. Another possible cause for the discrepancy between these results and the previous results with α-GalCer alone is that the α-GalCer is a difficult molecule to produce and its limited solubility makes storage difficult. Thus, the molecule may have degraded before it could be conjugated to the SPIO nanoparticles. The most likely contributor in these conjugation challenges is the amine surface of the nanoparticle.

Therapy using our nanovaccine on mice indicated inhibition of tumor growth yet not at a robust level. Assessment of cytokine production after injection of the nanovaccine showed a complete absence of expected cytokines. This means that injection of our nanovaccine was unable to activate the expected immune response. This conclusion was supported by comparing cytokine expression with injection of the nanovaccine and soluble solutions. The soluble solutions elicited an immune response unlike the nanoparticle bound, an observation supporting the conclusion that conjugation of the biomolecules to SPIO nanoparticles was unsuccessful. While the therapy showed some promise in terms of tumor response, future therapy and cytokine measurements

should include additional positive and negative controls to facilitate a more robust interpretation of the results. Additionally, analytical chemistry and quality control must be utilized to ensure the presence of adjuvant and tumor antigen on the surface of the nanoparticles.

Nebulization has been identified as a means through which to accomplish the intrinsic presentation of antigenic molecules to DCs in the lungs. The first technique used for nebulization, through the nose of the animal, was mostly unsuccessful due to the imperfections of the nebulizing device. In many cases, the animal avoided breathing the aerosol since too much room was available within the containment chamber. The intubation of the mice for nebulization was more successful in delivering nanoparticles to the lungs as can be seen in the histology data, as well as optical imaging with the HINP. Histology of SPIO nanoparticles in the LN, as well as, optical imaging of HINP showed presence of nebulized nanoparticles in the mediastinal LNs. That data supports our hypothesis that lung DCs uptake the nebulized nanoparticles and migrate to the LN with the intracellular nanoparticles. The increased success of nebulization with the intubation technique was not without its drawbacks. The intubation process was found to be dangerous to the animal and the concentration of SPIO nanoparticles that was delivered to the lungs was not consistent across animals. Therefore, a new nebulizer was designed to simplify nebulization compared to the technique using intubation while keeping its advantage over the initial nebulization system.

The development of a NIR dye that can be conjugated onto biomolecules is desirable, especially as a molecular probe capable of being targeted to a certain place or process *in vivo*. NIR wavelengths are optimal for optical imaging due the low

absorbance and scattering of these wavelengths in tissue, which allows such dyes to be imaged up to a 1-2 centimeters into tissues. A commercial NIR dye was used for this study to focus on the activation of the dye rather than the synthesis of a new cyanine dye. It is worth mentioning that this synthesis was reported from the Pham Laboratory (Pham et al., 2008). The purpose of this work is to fine tune the chemistry for improving the dye's stability. The functionalization of the dye with aminoundecanoic acid to provide activation site in the carboxylic acid proceeds through an S_N2 nucleophilic substitution. Interestingly, this reaction produced a better yield in EtOH than DMF despite being a polar protic solvent. The reaction was carried out with relative ease due to microwave synthesis and purified with CombiFlash chromatography. The yield of this reaction was approximately 65%. The carboxylic acid can be activated with DCC and NHS to form a succinimidyl ester. This reaction proceeds in an oxygen-free environment and is monitored by the production of a precipitate byproduct. After filtering away the byproduct, the product can be purified with CombiFlash chromatography.

Bioconjugation of the NIR dye to PNA provides preliminary evidence towards the utility of a succinimide-activated NIR dye for optical imaging. Conjugation of the NIR dye is a simple process that can be easily repeated with a variety of targeting biomolecules.

The challenges and advances identified in these studies can be used for the future development of a nebulizing nanovaccine for cancer treatment. Given the robustness of optical imaging, a targetable NIR dye can help validate the use of such an approach.

Bibliography

Backman, V., M.B. Wallace, L.T. Perelman, J.T. Arendt, R. Gurjar, M.G. Muller, Q. Zhang, G. Zonios, E. Kline, J.A. McGilligan, S. Shapshay, T. Valdez, K. Badizadegan, J.M. Crawford, M. Fitzmaurice, S. Kabani, H.S. Levin, M. Seiler, R.R. Dasari, I. Itzkan, J. Van Dam, and M.S. Feld. 2000. Detection of preinvasive cancer cells. *Nature*. 406:35-36.

Banks, P.R., and D.M. Paquette. 1995. Comparison of three common amine reactive fluorescent probes used for conjugation to biomolecules by capillary zone electrophoresis. *Bioconjugate chemistry*. 6:447-458.

Bouvier, I., H. Jusforgues-Saklani, A. Lim, F. Lemaitre, B. Lemercier, C. Auriau, M.A. Nicola, S. Leroy, H.K. Law, A. Bandeira, J.J. Moon, P. Bousso, and M.L. Albert. 2011. Immunization route dictates cross-priming efficiency and impacts the optimal timing of adjuvant delivery. *Frontiers in immunology*. 2:71.

Brossart, P., S. Wirths, G. Stuhler, V.L. Reichardt, L. Kanz, and W. Brugger. 2000. Induction of cytotoxic T-lymphocyte responses in vivo after vaccinations with peptide-pulsed dendritic cells. *Blood*. 96:3102-3108.

Carlsson, J., H. Drevin, and R. Axen. 1978. Protein thiolation and reversible protein-protein conjugation. N-Succinimidyl 3-(2-pyridyldithio)propionate, a new heterobifunctional reagent. *The Biochemical journal*. 173:723-737.

Chang, D.H., K. Osman, J. Connolly, A. Kukreja, J. Krasovsky, M. Pack, A. Hutchinson, M. Geller, N. Liu, R. Annable, J. Shay, K. Kirchhoff, N. Nishi, Y. Ando, K. Hayashi, H. Hassoun, R.M. Steinman, and M.V. Dhodapkar. 2005. Sustained expansion of NKT cells and antigen-specific T cells after injection of alpha-galactosyl-ceramide loaded mature dendritic cells in cancer patients. *The Journal of experimental medicine*. 201:1503-1517.

Cheever, M.A., J.P. Allison, A.S. Ferris, O.J. Finn, B.M. Hastings, T.T. Hecht, I. Mellman, S.A. Prindiville, J.L. Viner, L.M. Weiner, and L.M. Matrisian. 2009. The prioritization of cancer antigens: a national cancer institute pilot project for the acceleration of translational research. *Clinical cancer research : an official journal of the American Association for Cancer Research*. 15:5323-5337.

de Vries, I.J., W.J. Lesterhuis, J.O. Barentsz, P. Verdijk, J.H. van Krieken, O.C. Boerman, W.J. Oyen, J.J. Bonenkamp, J.B. Boezeman, G.J. Adema, J.W. Bulte, T.W. Scheenen, C.J. Punt, A. Heerschap, and C.G. Figdor. 2005. Magnetic resonance tracking of dendritic cells in melanoma patients for monitoring of cellular therapy. *Nature biotechnology*. 23:1407-1413.

Dwyer, R.M., E.R. Bergert, M.K. O'Connor, S.J. Gendler, and J.C. Morris. 2006. Adenovirus-mediated and targeted expression of the sodium-iodide symporter permits in vivo radioiodide imaging and therapy of pancreatic tumors. *Human gene therapy*. 17:661-668.

Ema, H.S., T.; Miura, Y.; and Nakauchi H. 1990. Colony Formation of Clone-Sorted Human Hematopoietic Progenitors. *Blood*. 75:5.

Flamand, V., T. Sornasse, K. Thielemans, C. Demanet, M. Bakkus, H. Bazin, F. Tielemans, O. Leo, J. Urbain, and M. Moser. 1994. Murine dendritic cells pulsed in vitro with tumor antigen induce tumor resistance in vivo. *European journal of immunology*. 24:605-610.

Flanagan, J.H., Jr., S.H. Khan, S. Menchen, S.A. Soper, and R.P. Hammer. 1997. Functionalized tricarbocyanine dyes as near-infrared fluorescent probes for biomolecules. *Bioconjugate chemistry*. 8:751-756.

Fong, L., D. Brockstedt, C. Benike, L. Wu, and E.G. Engleman. 2001. Dendritic cells injected via different routes induce immunity in cancer patients. *Journal of immunology*. 166:4254-4259.

Franck, R.W., and M. Tsuji. 2006. Alpha-c-galactosylceramides: synthesis and immunology. *Accounts of chemical research*. 39:692-701.

Grabbe, S., S. Bruvers, R.L. Gallo, T.L. Knisely, R. Nazareno, and R.D. Granstein. 1991. Tumor antigen presentation by murine epidermal cells. *Journal of immunology*. 146:3656-3661.

Grolleau, A., A. Sloan, and J.J. Mule. 2005. Dendritic cell-based vaccines for cancer therapy. *Cancer treatment and research*. 123:181-205.

Harisinghani, M.G., J. Barentsz, P.F. Hahn, W.M. Deserno, S. Tabatabaei, C.H. van de Kaa, J. de la Rosette, and R. Weissleder. 2003. Noninvasive detection of clinically occult lymph-node metastases in prostate cancer. *The New England journal of medicine*. 348:2491-2499.

Hattrup, C.L., and S.J. Gendler. 2006. MUC1 alters oncogenic events and transcription in human breast cancer cells. *Breast cancer research : BCR*. 8:R37.

Hayakawa, Y., S. Rovero, G. Forni, and M.J. Smyth. 2003. Alpha-galactosylceramide (KRN7000) suppression of chemical- and oncogene-dependent carcinogenesis. *Proceedings of the National Academy of Sciences of the United States of America*. 100:9464-9469.

Hilderbrand, S.A., and R. Weissleder. 2010. Near-infrared fluorescence: application to in vivo molecular imaging. *Current opinion in chemical biology*. 14:71-79.

Hirosue, S., I.C. Kourtis, A.J. van der Vlies, J.A. Hubbell, and M.A. Swartz. 2010. Antigen delivery to dendritic cells by poly(propylene sulfide) nanoparticles with disulfide conjugated peptides: Cross-presentation and T cell activation. *Vaccine*. 28:7897-7906.

Holt, P.G., J. Oliver, N. Bilyk, C. McMenamin, P.G. McMenamin, G. Kraal, and T. Thepen. 1993. Downregulation of the antigen presenting cell function(s) of pulmonary dendritic cells in vivo by resident alveolar macrophages. *The Journal of experimental medicine*. 177:397-407.

Holtl, L., C. Rieser, C. Papesh, R. Ramoner, M. Herold, H. Klocker, C. Radmayr, A. Stenzl, G. Bartsch, and M. Thurnher. 1999. Cellular and humoral immune responses in patients with metastatic renal cell carcinoma after vaccination with antigen pulsed dendritic cells. *The Journal of urology*. 161:777-782.

Hsu, F.J., C. Benike, F. Fagnoni, T.M. Liles, D. Czerwinski, B. Taidi, E.G. Engleman, and R. Levy. 1996. Vaccination of patients with B-cell lymphoma using autologous antigen-pulsed dendritic cells. *Nature medicine*. 2:52-58.

Ito, T., M. Inaba, K. Inaba, J. Toki, S. Sogo, T. Iguchi, Y. Adachi, K. Yamaguchi, R. Amakawa, J. Valladeau, S. Saeland, S. Fukuhara, and S. Ikehara. 1999. A CD1a+/CD11c+ subset of human blood dendritic cells is a direct precursor of Langerhans cells. *Journal of immunology*. 163:1409-1419.

Jaffer, F.A., and R. Weissleder. 2005. Molecular imaging in the clinical arena. *JAMA : the journal of the American Medical Association*. 293:855-862.

Jemal, A., F. Bray, M.M. Center, J. Ferlay, E. Ward, and D. Forman. 2011. Global cancer statistics. *CA: a cancer journal for clinicians*. 61:69-90.

Kinlough, C.L., P.A. Poland, S.J. Gendler, P.E. Mattila, D. Mo, O.A. Weisz, and R.P. Hughey. 2011. Core-glycosylated mucin-like repeats from MUC1 are an apical targeting signal. *The Journal of biological chemistry*. 286:39072-39081.

Kobukai, S., R. Baheza, J.G. Cobb, J. Virostko, J. Xie, A. Gillman, D. Koktysh, D. Kerns, M. Does, J.C. Gore, and W. Pham. 2010. Magnetic nanoparticles for imaging dendritic cells. *Magnetic resonance in medicine : official journal of the Society of Magnetic Resonance in Medicine / Society of Magnetic Resonance in Medicine*. 63:1383-1390.

Kobukai, S., G.J. Kremers, J.G. Cobb, R. Baheza, J. Xie, A. Kuley, M. Zhu, and W. Pham. 2011. Induction of antitumor immunity by dendritic cells loaded with membrane-translocating mucin 1 Peptide antigen. *Translational oncology*. 4:1-8.

Koido, S., M. Kashiwaba, D. Chen, S. Gendler, D. Kufe, and J. Gong. 2000. Induction of antitumor immunity by vaccination of dendritic cells transfected with MUC1 RNA. *Journal of immunology*. 165:5713-5719.

Koktysh, D., V. Bright, and W. Pham. 2011. Fluorescent magnetic hybrid nanoprobe for multimodal bioimaging. *Nanotechnology*. 22:275606.

Kondo, H., S. Hazama, T. Kawaoka, S. Yoshino, S. Yoshida, K. Tokuno, M. Takashima, T. Ueno, Y. Hinoda, and M. Oka. 2008. Adoptive immunotherapy for pancreatic cancer using MUC1 peptide-pulsed dendritic cells and activated T lymphocytes. *Anticancer research*. 28:379-387.

Kugler, A., G. Stuhler, P. Walden, G. Zoller, A. Zobywalski, P. Brossart, U. Trefzer, S. Ullrich, C.A. Muller, V. Becker, A.J. Gross, B. Hemmerlein, L. Kanz, G.A. Muller, and R.H. Ringert. 2000. Regression of human metastatic renal cell carcinoma after vaccination with tumor cell-dendritic cell hybrids. *Nature medicine*. 6:332-336.

Lakshminarayanan, V., P. Thompson, M.A. Wolfert, T. Buskas, J.M. Bradley, L.B. Pathangey, C.S. Madsen, P.A. Cohen, S.J. Gendler, and G.J. Boons. 2012. Immune recognition of tumor-associated mucin MUC1 is achieved by a fully synthetic aberrantly glycosylated MUC1 tripartite vaccine. *Proceedings of the National Academy of Sciences of the United States of America*. 109:261-266.

Lambrecht, B.N., and H. Hammad. 2010. The role of dendritic and epithelial cells as master regulators of allergic airway inflammation. *Lancet*. 376:835-843.

Liu, S.Y.H., Y.; Yin, L. P.; Long, L.; Liu, R. 2008. Toxicology Studies of a Superparamagnetic iron oxide nanoparicle in vivo. *Advanced Materials Research (Volumes 47-50)*. Muti-functional Materials and Structures:1097-1100.

Liu, Y., R.D. Goff, D. Zhou, J. Mattner, B.A. Sullivan, A. Khurana, C. Cantu, 3rd, E.V. Ravkov, C.C. Ibegbu, J.D. Altman, L. Teyton, A. Bendelac, and P.B. Savage. 2006. A modified alpha-galactosyl ceramide for staining and stimulating natural killer T cells. *Journal of immunological methods*. 312:34-39.

Lodge, P.A., L.A. Jones, R.A. Bader, G.P. Murphy, and M.L. Salgaller. 2000. Dendritic cell-based immunotherapy of prostate cancer: immune monitoring of a phase II clinical trial. *Cancer research*. 60:829-833.

Martin-Fontecha, A., S. Sebastiani, U.E. Hopken, M. Uguccioni, M. Lipp, A. Lanzavecchia, and F. Sallusto. 2003. Regulation of dendritic cell migration to the draining lymph node: impact on T lymphocyte traffic and priming. *The Journal of experimental medicine*. 198:615-621.

Mayordomo, J.I., T. Zorina, W.J. Storkus, L. Zitvogel, C. Celluzzi, L.D. Falo, C.J. Melief, S.T. Ildstad, W.M. Kast, A.B. Deleo, and et al. 1995. Bone marrow-derived dendritic cells pulsed with synthetic tumour peptides elicit protective and therapeutic antitumour immunity. *Nature medicine*. 1:1297-1302.

Mohty, M., D. Olive, and B. Gaugler. 2002. Leukemic dendritic cells: potential for therapy and insights towards immune escape by leukemic blasts. *Leukemia :*

official journal of the Leukemia Society of America, Leukemia Research Fund, U.K. 16:2197-2204.

Morita, M., K. Motoki, K. Akimoto, T. Natori, T. Sakai, E. Sawa, K. Yamaji, Y. Koezuka, E. Kobayashi, and H. Fukushima. 1995. Structure-activity relationship of alpha-galactosylceramides against B16-bearing mice. *Journal of medicinal chemistry*. 38:2176-2187.

Mukherjee, P., C.S. Madsen, A.R. Ginardi, T.L. Tinder, F. Jacobs, J. Parker, B. Agrawal, B.M. Longenecker, and S.J. Gendler. 2003. Mucin 1-specific immunotherapy in a mouse model of spontaneous breast cancer. *Journal of immunotherapy*. 26:47-62.

Mukherjee, P., L.B. Pathangey, J.B. Bradley, T.L. Tinder, G.D. Basu, E.T. Akporiaye, and S.J. Gendler. 2007. MUC1-specific immune therapy generates a strong anti-tumor response in a MUC1-tolerant colon cancer model. *Vaccine*. 25:1607-1618.

Murphy, S.L.X., J.; Kochanek, K. D.;. 2012. Deaths: Preliminary Data for 2010. *National Vital Statistics Reports*. 60:1-51.

Nair, S.K., M. Morse, D. Boczkowski, R.I. Cumming, L. Vasovic, E. Gilboa, and H.K. Lyerly. 2002. Induction of tumor-specific cytotoxic T lymphocytes in cancer patients by autologous tumor RNA-transfected dendritic cells. *Annals of surgery*. 235:540-549.

Nembrini, C., A. Stano, K.Y. Dane, M. Ballester, A.J. van der Vlies, B.J. Marsland, M.A. Swartz, and J.A. Hubbell. 2011. Nanoparticle conjugation of antigen enhances cytotoxic T-cell responses in pulmonary vaccination. *Proceedings of the National Academy of Sciences of the United States of America*. 108:E989-997.

Nickels, M., J. Xie, J. Cobb, J.C. Gore, and W. Pham. 2010. Functionalization of iron oxide nanoparticles with a versatile epoxy amine linker. *Journal of materials chemistry*. 20:4776-4780.

Nolting, D.D.; Nickels, M.L.; Guo, N.; Pham, W. 2012. Molecular imaging probe development. *Am J Nucl Med Mol Imaging*. 2:273-306.

Ntziachristos, V., C. Bremer, and R. Weissleder. 2003. Fluorescence imaging with near-infrared light: new technological advances that enable in vivo molecular imaging. *European radiology*. 13:195-208.

Pecher, G., A. Haring, L. Kaiser, and E. Thiel. 2002. Mucin gene (MUC1) transfected dendritic cells as vaccine: results of a phase I/II clinical trial. *Cancer immunology, immunotherapy : CII*. 51:669-673.

Pham, W., L. Cassell, A. Gillman, D. Koktysh, and J.C. Gore. 2008. A near-infrared dye for multichannel imaging. *Chem Commun (Camb)*:1895-1897.

Pham, W., S. Kobukai, C. Hotta, and J.C. Gore. 2009. Dendritic cells: therapy and imaging. *Expert opinion on biological therapy*. 9:539-564.

Pham, W., Z. Medarova, and A. Moore. 2005. Synthesis and application of a water-soluble near-infrared dye for cancer detection using optical imaging. *Bioconjugate chemistry*. 16:735-740.

Pham, W., J. Xie, and J.C. Gore. 2007. Tracking the migration of dendritic cells by in vivo optical imaging. *Neoplasia*. 9:1130-1137.

Pinkhasov, J., M.L. Alvarez, M.M. Rigano, K. Piensook, D. Larios, M. Pabst, J. Grass, P. Mukherjee, S.J. Gendler, A.M. Walmsley, and H.S. Mason. 2011. Recombinant plant-expressed tumour-associated MUC1 peptide is immunogenic and capable of breaking tolerance in MUC1.Tg mice. *Plant biotechnology journal*. 9:991-1001.

Porgador, A., D. Snyder, and E. Gilboa. 1996. Induction of antitumor immunity using bone marrow-generated dendritic cells. *Journal of immunology*. 156:2918-2926.

Rebizak, R., M. Schaefer, and E. Dellacherie. 1997. Polymeric conjugates of Gd(3+)-diethylenetriaminepentaacetic acid and dextran. 1. Synthesis, characterization, and paramagnetic properties. *Bioconjugate chemistry*. 8:605-610.

Reddy, S.T., A.J. van der Vlies, E. Simeoni, V. Angeli, G.J. Randolph, C.P. O'Neil, L.K. Lee, M.A. Swartz, and J.A. Hubbell. 2007. Exploiting lymphatic transport and complement activation in nanoparticle vaccines. *Nature biotechnology*. 25:1159-1164.

Sadanaga, N., H. Nagashima, K. Mashino, K. Tahara, H. Yamaguchi, M. Ohta, T. Fujie, F. Tanaka, H. Inoue, K. Takesako, T. Akiyoshi, and M. Mori. 2001. Dendritic cell vaccination with MAGE peptide is a novel therapeutic approach for gastrointestinal carcinomas. *Clinical cancer research : an official journal of the American Association for Cancer Research*. 7:2277-2284.

Seitz, R.C., K. Fischer, H.E. Stegner, and A. Poschmann. 1984. Detection of metastatic breast carcinoma cells by immunofluorescent demonstration of Thomsen-Friedenreich antigen. *Cancer*. 54:830-836.

Sertl, K., T. Takemura, E. Tschachler, V.J. Ferrans, M.A. Kaliner, and E.M. Shevach. 1986. Dendritic cells with antigen-presenting capability reside in airway epithelium, lung parenchyma, and visceral pleura. *The Journal of experimental medicine*. 163:436-451.

Shysh, A., S.M. Eu, A.A. Noujaim, M.R. Suresh, and B.M. Longenecker. 1985. Radioimmunodetection of murine mammary adenocarcinoma (TA3/Ha) lung and liver metastases with radioiodinated PNA. *International journal of cancer. Journal international du cancer*. 35:113-119.

Siegel, R., E. Ward, O. Brawley, and A. Jemal. 2011. Cancer statistics, 2011: the impact of eliminating socioeconomic and racial disparities on premature cancer deaths. *CA: a cancer journal for clinicians*. 61:212-236.

Sou, T., E.N. Meeusen, M. de Veer, D.A. Morton, L.M. Kaminskas, and M.P. McIntosh. 2011. New developments in dry powder pulmonary vaccine delivery. *Trends in biotechnology*. 29:191-198.

Steinman, R.M., and Z.A. Cohn. 1973. Identification of a novel cell type in peripheral lymphoid organs of mice. I. Morphology, quantitation, tissue distribution. *The Journal of experimental medicine*. 137:1142-1162.

Steinman, R.M., and M.C. Nussenzweig. 1980. Dendritic cells: features and functions. *Immunological reviews*. 53:127-147.

Sullivan, B.A., and M. Kronenberg. 2005. Activation or anergy: NKT cells are stunned by alpha-galactosylceramide. *The Journal of clinical investigation*. 115:2328-2329.

Taylor-Papadimitriou, J., J. Burchell, D.W. Miles, and M. Dalziel. 1999. MUC1 and cancer. *Biochimica et biophysica acta*. 1455:301-313.

Thapa, P., G. Zhang, C. Xia, A. Gelbard, W.W. Overwijk, C. Liu, P. Hwu, D.Z. Chang, A. Courtney, J.K. Sastry, P.G. Wang, C. Li, and D. Zhou. 2009. Nanoparticle formulated alpha-galactosylceramide activates NKT cells without inducing anergy. *Vaccine*. 27:3484-3488.

Thurner, B., I. Haendle, C. Roder, D. Dieckmann, P. Keikavoussi, H. Jonuleit, A. Bender, C. Maczek, D. Schreiner, P. von den Driesch, E.B. Brocker, R.M. Steinman, A. Enk, E. Kampgen, and G. Schuler. 1999. Vaccination with mage-3A1 peptide-pulsed mature, monocyte-derived dendritic cells expands specific cytotoxic T cells and induces regression of some metastases in advanced stage IV melanoma. *The Journal of experimental medicine*. 190:1669-1678.

van der Vlies, A.J., C.P. O'Neil, U. Hasegawa, N. Hammond, and J.A. Hubbell. 2010. Synthesis of pyridyl disulfide-functionalized nanoparticles for conjugating thiol-containing small molecules, peptides, and proteins. *Bioconjugate chemistry*. 21:653-662.

Vlad, A.M., J.C. Kettel, N.M. Alajez, C.A. Carlos, and O.J. Finn. 2004. MUC1 immunobiology: from discovery to clinical applications. *Advances in immunology*. 82:249-293.

Weissleder, R. 2006. Molecular imaging in cancer. *Science*. 312:1168-1171.

Wierecky, J., M. Mueller, and P. Brossart. 2006. Dendritic cell-based cancer immunotherapy targeting MUC-1. *Cancer immunology, immunotherapy : CII*. 55:63-67.

Winer, J.L., C.Y. Liu, and M.L. Apuzzo. 2011. The Use of Nanoparticles as Contrast Media in Neuroimaging: A Statement on Toxicity. *World neurosurgery*.

Winzler, C., P. Rovere, M. Rescigno, F. Granucci, G. Penna, L. Adorini, V.S. Zimmermann, J. Davoust, and P. Ricciardi-Castagnoli. 1997. Maturation stages of mouse dendritic cells in growth factor-dependent long-term cultures. *The Journal of experimental medicine*. 185:317-328.

Zhou, X.T., C. Forestier, R.D. Goff, C. Li, L. Teyton, A. Bendelac, and P.B. Savage. 2002. Synthesis and NKT cell stimulating properties of fluorophore- and biotin-appended 6"-amino-6"-deoxy-galactosylceramides. *Organic letters*. 4:1267-1270.